

No-boundary extremal surfaces in slow-roll inflation and other cosmologies

Kaberi Goswami, K. Narayan, Gopal Yadav

*Chennai Mathematical Institute,
H1 SIPCOT IT Park, Siruseri 603103, India.*

Abstract

Building on previous work on de Sitter extremal surfaces anchored at the future boundary, we study no-boundary extremal surfaces in slow-roll inflation models, with perturbations to no-boundary global dS preserving the spatial isometry. While in pure de Sitter space the Euclidean hemisphere gives a real area equalling half de Sitter entropy, the no-boundary extremal surface areas here have nontrivial real and imaginary pieces overall. We evaluate the area integrals in the complex time-plane defining appropriate contours. For the 4-dim case, the real and imaginary finite corrections at leading order in the slow-roll parameter match those in the semiclassical expansion of the Wavefunction (or action), and corroborate the cosmic brane interpretation discussed previously. We also study no-boundary extremal surfaces in other cosmologies including 3-dimensional inflation and Schwarzschild de Sitter spaces with small mass.

Contents

1	Introduction	1
2	Reviewing de Sitter extremal surfaces	4
3	Slow-roll inflation, no-boundary extremal surfaces	7
3.1	dS_4 area including $O(\epsilon)$ correction	10
4	Other cosmologies	14
4.1	dS_3 area including $O(\epsilon)$ correction	14
4.2	Schwarzschild de Sitter black holes with small mass	16
4.2.1	Extremal dS_4 : Nariai	18
4.3	FRW+slow-roll cosmologies	19
5	Discussion	19
A	The basic setup on inflation	22
A.1	dS_4 slow roll	22
A.2	dS_3 slow roll	24
B	Details: dS_4 slow-roll area	24
C	Details: dS_3 slow-roll area	26
D	Inflation: on-shell action etc	28

1 Introduction

It is of great interest to understand cosmology from the point of view of holography [1, 2, 3]. One of the many fascinating aspects of our understanding of holography in AdS -like spaces is the Ryu-Takayanagi formulation of holographic entanglement entropy [4, 5, 6, 7] and its many ramifications. Towards exploring these quantum information ideas in cosmological contexts, it is fascinating to look at de Sitter space as a idealized example of cosmology. This however already has many new features. Thinking of time as the holographic direction, a natural boundary for de Sitter space is in the far future (or past), leading to dS/CFT [8, 9, 10, 11] (see *e.g.* [12, 13, 14] for reviews on de Sitter space and its entropy [15]).

Certain generalizations of the Ryu-Takayanagi formulation of AdS holographic entanglement to de Sitter space were studied in [16, 17, 18, 19, 20, 21, 22, 23, 24, 25]. These pertain to RT/HRT extremal surfaces anchored at the dS future boundary I^+ and amount to considering the bulk analog of setting up entanglement entropy in the dual CFT at I^+ , in part towards understanding if de Sitter entropy [15] can be understood as some sort of holographic entanglement entropy. Analysing the extremization shows that surfaces anchored at I^+ do not return to I^+ . In entirely Lorentzian dS , this leads to future-past timelike surfaces stretching between I^\pm with pure imaginary area. With a no-boundary type Hartle-Hawking boundary condition, the top half of these timelike surfaces joins with a spacelike part on the hemisphere giving a complex-valued area [23], [24] (and [26, 27] for dS_3/CFT_2). The real part of the area arises from the hemisphere and is precisely half de Sitter entropy (Figure 1). Some of these structures [20, 21, 22] are akin to space-time rotations from AdS (some related

discussions appear in [28]). In [25], certain analytic continuations were discussed which in fact amount to space-time rotations from AdS .

Recent investigations suggest that the areas of these extremal surfaces are best interpreted as encoding pseudo-entropy or time-entanglement [23], [24], entanglement-like structures involving timelike separations. Pseudo-entropy [29] is the entropy based on the transition matrix $|f\rangle\langle i|$ regarded as a generalized density operator (see also [30]-[42] for some partially related work). In some sense this is perhaps the natural object here since the absence of $I^+ \rightarrow I^+$ returns for extremal surfaces suggests that extra data is required in the interior, somewhat reminiscent of scattering amplitudes (equivalently the time evolution operator), and of [9] viewing de Sitter space as a collection of past-future amplitudes. This is also suggested by the dS/CFT dictionary $Z_{CFT} = \Psi_{dS}$ [10]: boundary “entanglement entropy” formulated via Z_{CFT} translates to a bulk object formulated via the Wavefunction Ψ_{dS} (a single ket, rather than a density matrix), leading (not surprisingly) to non-hermitian structures. In [25], fuelled by the analytic continuation, a heuristic version of the Lewkowycz-Maldacena argument [43, 44, 45, 46] (see also [47]) was constructed for the no-boundary de Sitter extremal surfaces for maximal (IR) subregions. Roughly the boundary replica argument on Z_{CFT} translates now to a bulk replica argument on the Wavefunction Ψ_{dS} which is essentially pseudo-entropy. The area now is interpreted as the amplitude for creation of a cosmic brane that localizes on the part Euclidean, part timelike no-boundary extremal surface.

In this paper, we study no-boundary extremal surfaces¹ in slow-roll inflation models, with certain inflationary cosmological perturbations to no-boundary de Sitter space which preserve the spatial spherical isometry of dS in global coordinates. These perturbations are described by scalar inflaton perturbations defined imposing regularity at the no-boundary point: this induces corresponding metric perturbations as well (see Figure 2). The perturbations have explicit analytic (although still adequately complicated) expressions to $O(\epsilon)$ in the slow-roll parameter ϵ , as described in [49] (and related previous work *e.g.* [48]-[57] that we found useful). This allows us to perform explicit analytic calculations of the no-boundary extremal surface areas and compare them with the Wavefunction. As in de Sitter, we consider maximal (IR) subregions on equatorial plane slices regarded as boundary Euclidean time slices, and look for codim-2 extremal surfaces dipping into the bulk time direction. These are, mostly, entirely timelike in the top Lorentzian part, going around the Euclidean hemisphere. However now the inflationary perturbations induce small wiggles around pure de Sitter, so the metric has various interesting real and imaginary pieces. Thus the no-

¹The phrase “no-boundary extremal surface” refers to the Hartle-Hawking type nature of these surfaces in no-boundary de Sitter space [48], not to be confused with the fact that the surfaces are anchored at an asymptotic (future) boundary. Similar comments apply to the no-boundary slow-roll inflation studies here.

boundary extremal surface areas now have nontrivial real and imaginary pieces which now arise from both the Euclidean hemisphere and the Lorentzian timelike regions. In general it turns out that the corresponding area integrals must be regarded carefully in the complex time-plane defining appropriate contours (Figure 3) that avoid extra poles at the complexification point that arise from the slow-roll perturbations (similar in spirit to calculations of the semiclassical Wavefunction of the Universe). Doing this carefully, we eventually find divergent pure imaginary pieces from near the future boundary as well as real and imaginary finite slow-roll corrections to the leading half de Sitter entropy $\frac{\pi l^2}{2G_4}$ contribution from the hemisphere. For example, we obtain (22) in dS_4 slow-roll inflation with the finite parts being $\frac{\pi l^2}{2G_4} (1 + \epsilon (\log 4 - \frac{7}{2} + i\pi))$. These finite $O(\epsilon)$ corrections precisely match the finite $O(\epsilon)$ corrections in the expansion of the semiclassical Wavefunction of the Universe (equivalently the on-shell action) in slow-roll inflation described in [49]. This is consistent with the Lewkowycz-Maldacena interpretation in [25] of these no-boundary extremal surface areas giving the probability for cosmic brane creation but now in the slow-roll no-boundary geometry.

We do a similar calculation for dS_3 slow-roll inflation as well, with similar spatial spherical symmetry preserving inflaton perturbations and corresponding metric ones. The no-boundary extremal surface areas again have real and imaginary slow-roll corrections. We find that the real finite $O(\epsilon)$ corrections again match those in the expansion of semiclassical Wavefunction (or on-shell action), but the imaginary finite parts do not match. This is likely due to the fact that the boundary reflects a CFT on an even dimensional sphere, with potential extra pure imaginary terms that arise from anomalies. The probabilities, controlled by the real parts, match.

To put this in perspective, it is worth recalling the behaviour of minimal RT surfaces in the AdS black hole [4, 5]. As the boundary subregion size increases, the RT surface dips deeper into the bulk and in the IR limit (maximal subregion), the surface wraps the black hole horizon. The finite part of holographic entanglement entropy then becomes black hole entropy which is the thermal entropy of the dual field theory: this entropy can also be realized from the on-shell action regarded as a partition function [58] (see also [59, 60]). In the de Sitter case with surfaces anchored at the future boundary, the only turning points are in the Euclidean hemisphere which then gives half de Sitter entropy as the real finite part of the no-boundary extremal surface area (in particular for maximal (IR) subregions). This can also be realized by evaluating the on-shell action (semiclassical Wavefunction Ψ_{dS}): the real part then gives the probability $|\Psi_{dS}|^2$ controlled by de Sitter entropy. The underlying reason here in dS stems from the Lewkowycz-Maldacena cosmic brane interpretation in [25]. In the context of slow-roll inflation, the perturbations mix everything but the cosmic brane

creation probability controlled by the real finite parts of the no-boundary areas continues to match the probability from the Wavefunction, corroborating the replica arguments near de Sitter. Both probabilities are controlled by de Sitter entropy and its slow-roll corrections, which is the maximum amount of “stuff” in the space.

We also study Schwarzschild de Sitter black holes which in general have conical singularities at the black hole and cosmological horizons which have different time periodicities. In the limit of small mass regarded as a perturbation, we define an appropriate no-boundary geometry at the cosmological horizon whose location is shifted by the black hole mass. Now the no-boundary extremal surface area is similar to that in de Sitter space with a reduced cosmological scale, with the real hemisphere contribution being half the entropy for the modified de Sitter space.

We review de Sitter extremal surfaces in sec. 2. The slow-roll inflation extremal surfaces appear in sec. 3 and sec. 3.1 for the dS_4 case, and sec. 4.1 for the dS_3 case. We then discuss Schwarzschild de Sitter in sec. 4.2 and FRW+slowroll cosmologies briefly in sec. 4.3. Sec. 5 contains a Discussion. Various details appear in the Appendices, in sec. A.1 and sec. A.2 on the inflation setup broadly, in sec. B and sec. C on the area calculation, and in sec. D on the Wavefunction/action.

2 Reviewing de Sitter extremal surfaces

We briefly review [24, 25] and previous work here on generalizations of RT/HRT extremal surfaces to de Sitter space (see also [23]). These involve considering the bulk analog of setting up entanglement entropy in the dual Euclidean *CFT* on the future boundary [16], restricting to some boundary Euclidean time slice, defining subregions on these, and looking for extremal surfaces anchored at I^+ dipping into the time (holographic) direction. Analysing this shows that there are no spacelike surfaces connecting points on I^+ . In entirely Lorentzian dS , there are future-past timelike surfaces stretching between I^\pm [20, 22], akin to rotated analogs of the Hartman-Maldacena surfaces [61] in the eternal *AdS* black hole [62]: these have pure imaginary area, relative to *AdS* spacelike RT/HRT surfaces. With a no-boundary type Hartle-Hawking boundary condition, the top half of these timelike surfaces joins with a spacelike part on the hemisphere giving a complex-valued area [23], [24] (and [26, 27] for dS_3/CFT_2). The real part of the area arises from the hemisphere and is precisely half de Sitter entropy. Due to the presence of timelike components in these extremal surfaces, these areas are best interpreted as pseudo-entropy, as we see below. From the dual side, in various toy models of “entanglement entropy” in ghost-like theories, complex-valued entropies arise naturally [63, 64] (see also [65]): the negative norm states here lead to imaginary components.

It is worth noting that the adjoints of states are nontrivial in such ghost-like theories so these are perhaps more correctly thought of as pseudo-entropy.

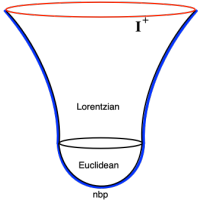


Figure 1: No-boundary de Sitter space, with the top Lorentzian region continuing smoothly into the Euclidean hemisphere region ending at the no-boundary point. Also shown are IR no-boundary extremal surfaces (blue) anchored at the future boundary I^+ dipping into the time direction, timelike in the Lorentzian region and going around the hemisphere.

These dS extremal surfaces can also be realized via analytic continuations from AdS (reviewed below). This suggests a natural way to obtain the no-boundary de Sitter extremal surface areas through a heuristic replica argument [25] involving an analytic continuation of the Lewkowycz-Maldacena formulation [43] in AdS to derive RT entanglement entropy (generalized in [44], [45], [46]; see also [47] and the review [7]). The crucial difference here is that since the analytic continuation maps Z_{bulk}^{AdS} to the de Sitter Wavefunction Ψ_{dS} , this is now a replica formulation on Ψ_{dS} , considering the dS/CFT dictionary $Z_{CFT} = \Psi_{dS}$ [10]. With the Wavefunction Ψ_{dS} regarded as an amplitude (or transition matrix from “nothing”), this gives pseudo-entropy. In particular the codim-2 brane that smooths out bulk (orbifold) singularities is now a time-evolving, part Euclidean, part timelike, brane. This gives a complex area semiclassically, with the real part from the Euclidean hemisphere and the timelike part pure imaginary. In this Lewkowycz-Maldacena formulation, the area of these no-boundary dS extremal surfaces arises as the amplitude for cosmic brane creation. So it is important that the divergent pieces of the area arising from near the future boundary are pure imaginary, since otherwise this amplitude would diverge. As it is, there is a finite probability: the real part arises from the maximal hemisphere, with size set by dS entropy.

Overall, directly analysing the bulk extremization and calculating the no-boundary extremal surface areas for the IR (maximal) subregions at the future boundary gives

$$(dS_4) \quad S_{nb} = -i \frac{\pi l^2}{2G_4} \frac{R_c}{l} + \frac{\pi l^2}{2G_4}; \quad (dS_3) \quad S_{nb} = -i \frac{l}{2G_3} \log \frac{R_c}{l} + \frac{\pi l}{4G_3}, \quad (1)$$

with the pure imaginary piece from the top Lorentzian part of dS and the real piece (precisely half de Sitter entropy) from the Euclidean hemisphere. These can also be realized via analytic continuations from the AdS RT surfaces which all lie on a constant time slice. Under the $dS \leftrightarrow AdS$ analytic continuation, this AdS constant time slice continues to dS as

$$\begin{aligned} ds_{(r>L)}^2 &= \frac{dr^2}{1 + \frac{r^2}{L^2}} + r^2 d\Omega_{d-1}^2 & \xrightarrow{L \rightarrow -il} & ds_{(r>l)}^2 = -\frac{dr^2}{\frac{r^2}{l^2} - 1} + r^2 d\Omega_{d-1}^2, \\ ds_{(r<L)}^2 &= \frac{dr^2}{1 + \frac{r^2}{L^2}} + r^2 d\Omega_{d-1}^2 & \xrightarrow{L \rightarrow -il} & ds_{(r<l)}^2 = \frac{dr^2}{1 - \frac{r^2}{l^2}} + r^2 d\Omega_{d-1}^2. \end{aligned} \quad (2)$$

The AdS boundary at $r \rightarrow \infty$ maps to the dS future boundary I^+ at $r \rightarrow \infty$, and the AdS region $r \in [L, \infty]$ maps to the dS future universe F parametrized by $r \in [l, \infty]$ (and r is time here). The dS hemisphere is $\tau_E = -it = [0, \frac{\pi}{2}]$ where $-\frac{dr^2}{\frac{r^2}{l^2} - 1} > 0$ is Euclidean.

The global dS_{d+1} metric with S^d cross-sections, restricted to any equatorial S^d plane is identical to the $t = const$ slice of the (Lorentzian) dS static coordinatization (2), above:

$$ds_{global}^2 \Big|_{\theta_d=const} = -d\tau^2 + l^2 \cosh^2 \frac{\tau}{l} d\Omega_{d-1}^2 = -\frac{dr^2}{\frac{r^2}{l^2} - 1} + r^2 d\Omega_{d-1}^2 = ds_{static}^2 \Big|_{t=const}, \quad (3)$$

using $r = l \cosh \frac{\tau}{l}$. Thus a generic equatorial plane in global dS defines the same boundary Euclidean time slice as the $t = const$ slice in the dS static coordinatization, and we will continue to use the parametrization (2).

The IR AdS surface space spans the entire AdS boundary sphere. This continues to the IR dS extremal surface (when the subregion becomes the whole space at I^+), going from $r \rightarrow \infty$ to $r = l$ as a timelike surface in the Lorentzian dS region and then in the hemisphere from $r = l$ to $r = r_* = 0$ (where it turns around). The turning point r_* only exists in the Euclidean (hemisphere) part of dS .

This IR surface starts at the boundary of the maximal subregion of the S^{d-1} (*i.e.* hemisphere) so it is anchored on the equator of the S^{d-1} (red curve in Figure 1) and wraps the equatorial S^{d-2} . From (2), it is clear that the IR dS extremal surface becomes a space-time rotation of that in AdS . Its area continues as (with R_c a cutoff at large r)

$$\begin{aligned} \frac{V_{S^{d-2}}}{4G_{d+1}} \int_0^{R_c} \frac{r^{d-2} dr}{\sqrt{1 + \frac{r^2}{L^2}}} &\xrightarrow{L \rightarrow -il} \frac{V_{S^{d-2}}}{4G_{d+1}} \int_0^l \frac{r^{d-2} dr}{\sqrt{1 - \frac{r^2}{l^2}}} + \frac{V_{S^{d-2}}}{4G_{d+1}} \int_l^{R_c} r^{d-2} \sqrt{\frac{dr^2}{-(\frac{r^2}{l^2} - 1)}}, \\ &= \frac{1}{2} \frac{l^{d-1} V_{S^{d-1}}}{4G_{d+1}} - i \# \frac{l^{d-1}}{4G_{d+1}} \frac{R_c^{d-2}}{l^{d-2}} + \dots \end{aligned} \quad (4)$$

where the \dots are subleading imaginary terms. For $AdS_4 \rightarrow dS_4$ and $AdS_3 \rightarrow dS_3$, we obtain

$$\frac{V_{S^1}}{4G_4} \int_0^{R_c} \frac{r dr}{\sqrt{1 + \frac{r^2}{L^2}}} = \frac{\pi L^2}{2G_4} \left(\frac{R_c}{L} - 1 \right) \rightarrow -i \frac{\pi l^2}{2G_4} \frac{R_c}{l} + \frac{\pi l^2}{2G_4} = S_{dS_4}^{IR}, \quad (5)$$

$$\frac{V_{S^0}}{4G_3} \int_0^{R_c} \frac{dr}{\sqrt{1 + \frac{r^2}{L^2}}} = \frac{2L}{4G_3} \log \frac{R_c}{L} \rightarrow -i \frac{l}{2G_3} \log \frac{R_c}{l} + \frac{\pi l}{4G_3} = S_{dS_3}^{IR}. \quad (6)$$

These extremal surfaces can also be described explicitly in dS_3 for more general boundary subregions (and for near maximal subregions in dS_{d+1}). Drawing out the extremal surfaces geometrically leads to a natural geometric identification of the bulk subregion dual to a boundary subregion as an appropriate ‘‘pseudo-entanglement’’ wedge defined as the appropriate domain of dependence bounded by the boundary subregion at I^+ and the extremal

surface. However it is *only* for maximal subregions that this leads to consistent disjoint bulk subregions corresponding to disjoint boundary subregions, and thereby a version of subregion-subregion duality. Thus maximal (IR) subregions appear to be the only well-defined subregions geometrically from the perspective of subregion duality.

3 Slow-roll inflation, no-boundary extremal surfaces

We will now describe no-boundary extremal surfaces in slow-roll inflation, with the leading dS_4 area corrected to $O(\epsilon)$ in the slow roll parameter. We first describe the basic setup, which is essentially that described in [49] (and related previous work *e.g.* [48]-[57] that we found useful). The spacetime metric near global dS_{d+1} is

$$ds^2 = -dt^2 + a(t)^2 d\Omega_d^2 = g_{aa} da^2 + a^2 d\Omega_d^2, \quad (7)$$

where we have redefined the time coordinate to be a in the second expression, which turns out to be convenient for our purposes. This form of the metric component g_{aa} applies for both the Euclidean and Lorentzian regions of the spacetime. For pure de Sitter in the above global coordinates, we have in the Lorentzian region $r > 1$,

$$a(t) = l \cosh \tau \equiv l r, \quad \tau = \frac{t}{l}, \quad g_{aa} = \frac{1}{1 - r^2} < 0. \quad (8)$$

The region $r < 1$ gives $g_{aa} > 0$ and describes the Euclidean hemisphere. A global S^d equatorial plane slice as a boundary Euclidean time slice then resembles the $t = \text{const}$ slice in dS static coordinatization, as in (3). The coordinate r here is essentially α in [49].

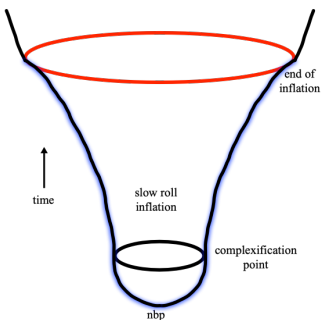


Figure 2: Slow-roll inflation as small perturbation wiggles about no-boundary de Sitter space. The Lorentzian region continues smoothly at the “complexification point” into the no-boundary hemisphere region ending at the no-boundary point. Inflation ends at the future boundary (the reheating surface), continuing with standard Big-Bang cosmology at later times. Also shown is the no-boundary extremal surface (blue shadow).

We now describe slow-roll inflationary perturbations about de Sitter space (Figure 2): the basic setup is in Appendix A.1 for the dS_4 case, reviewing the description in [49]. The inflaton scalar field ϕ rolls slowly down the potential $V(\phi)$, with a small slow-roll parameter $\epsilon = \frac{V'^2}{2V^2} \ll 1$. We use the Einstein-scalar equations to solve for the inflaton perturbation

profile to $O(\epsilon)$ and thereby the metric correction to that order (general useful reviews on inflation include [66, 67]).

Then the metric component g_{rr} to $O(\epsilon)$ in the slow-roll correction has the form

$$g_{aa} = \frac{1}{1-r^2} (1 + 2\epsilon \beta_{>}(r)), \quad (9)$$

where the slow roll correction $\beta_{>}(r)$ is a function of the rolling inflaton profile: we will describe this in detail later. The no-boundary extremal surfaces we are interested in lie on boundary Euclidean time slices taken as some S^d equatorial plane (*i.e.* S^{d-1}) and extend out from the S^{d-2} boundary of the maximal (hemisphere) subregion on this slice, as in the pure dS case: they thus wrap this S^{d-2} and extend in the time direction, making up the codim-2 surface (blue shadow in Figure 2). The metric corrections here have complicated functional form and lead to interesting corrections to the area as we will see. Since the inflationary perturbations here preserve the S^d spherical symmetry, the extremal surfaces on all such equatorial plane slices are equivalent.

The IR no-boundary extremal surface area is given by

$$\begin{aligned} S_{sr_{d+1}} &= S_{d+1}^{r<1} + S_{d+1}^{r>1} \\ &= \frac{V_{S^{d-2}} l^{d-1}}{4G_{d+1}} \left(\int_0^1 \frac{r^{d-2} \sqrt{1+2\epsilon\beta_{<}(r)}}{\sqrt{1-r^2}} dr + (-i) \int_1^{R_c/l} \frac{r^{d-2} \sqrt{1+2\epsilon\beta_{>}(r)}}{\sqrt{r^2-1}} dr \right) \end{aligned} \quad (10)$$

with the leading dS_{d+1} piece and the $O(\epsilon)$ slow roll correction, where $\beta_{<}(r)$ is to be obtained by analytically continuing $\beta_{>}(r)$ in the Lorentzian region $r > 1$ to the hemisphere region where $r < 1$. Expanding to $O(\epsilon)$ we obtain the first slow-roll correction to dS_4 and dS_3 as

$$S_{sr_4} \simeq \frac{\pi l^2}{2G_4} \left(-i \int_1^{R_c/l} \frac{1+\epsilon\beta_{>}(r)}{\sqrt{r^2-1}} r dr + \int_0^1 \frac{1+\epsilon\beta_{<}(r)}{\sqrt{1-r^2}} r dr \right) \quad (11)$$

$$S_{sr_3} \simeq \frac{l}{2G_3} \left(-i \int_1^{R_c/l} \frac{1+\epsilon\beta_{>}(r)}{\sqrt{r^2-1}} dr + \int_0^1 \frac{1+\epsilon\beta_{<}(r)}{\sqrt{1-r^2}} dr \right). \quad (12)$$

Towards evaluating this, note that the metric (9) at leading order $O(\epsilon^0)$ (*i.e.* pure de Sitter) already has a pole at $r = 1$ which is the complexification point where we transit from Lorentzian to Euclidean signature (this is $\tau = 0$, using (8)). This does not however lead to any singularities in the extremal surface areas: from (11), (12), the contribution near $r = 1$ is $\int \frac{dr}{\sqrt{\pm(1-r)}} \sim \sqrt{1-r}$ which is nonsingular, resulting in (4), (5), (6). However, when this pole leads to singularities in calculations, we should go around the pole avoiding it, *i.e.* in the upper half plane: this defines the contour in Figure 3 in the τ - or r -variables.

Considering the $O(\epsilon)$ slow-roll corrections, there are indeed extra singular terms in the above expressions (11), (12), at the complexification point $r = 1$, stemming from the extra

$\beta(r)$ terms in the integrand (see (19), sourced by the inflaton profile (17), using (16)). These extra poles lead to divergences, similar technically to those from poles occurring in other calculations in slow-roll inflation: see *e.g.* [49] for some discussions on this (including aspects of earlier numerical studies involving complex contours in the upper half plane avoiding the pole; see *e.g.* [57]). Note that since we are regarding the spacetime background here essentially as a near dS background in the slow-roll phase to $O(\epsilon)$, the details of the full inflationary solution (and the detailed form of the inflaton potential) are not important: thus the pole above necessarily remains in the $O(\epsilon)$ discussions here and must be dealt with.

In the current context, to define the extremal surface areas correctly, we must therefore define these areas as complex integrals in the complex time-plane, with a contour chosen to avoid the pole at $r = 1$, by going around it in the upper half plane, as in Figure 3 stated above. As long as we define the complex time-plane integral correctly, normalizing it so that the leading expressions are consistent with the leading de Sitter areas, the details of the contour around the pole are not important as we will see. In pure de Sitter, this time contour essentially encodes the geometric picture of time and correspondingly the shape of the IR extremal surface as in Figure 1. In slow-roll, since we are in the semiclassical regime near de Sitter, we expect that the time contour in our $O(\epsilon)$ slow-roll case should retain this semiclassical geometric picture of time and reflect the shape of the slow-roll extremal surface in Figure 2 as small wiggles near the de Sitter one.

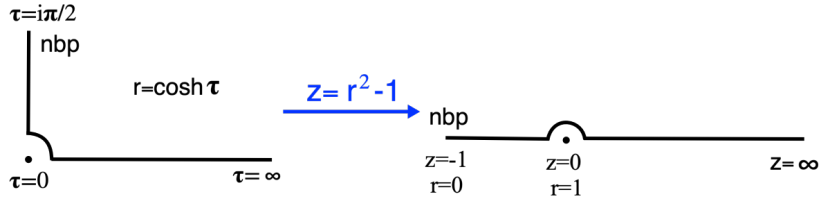


Figure 3: The time coordinate τ defines the contour on the left, from the no-boundary point in the Euclidean region at $\tau = i\frac{\pi}{2}$ to the complexification point at $\tau = 0$ and thereon to the Lorentzian region with real τ going to the future boundary $\tau \rightarrow \infty$. With the coordinate $r = \cosh \tau$ the nbp is $r = 0$ and the complexification point at $r = 1$. In terms of the coordinate $z = r^2 - 1$ we have the nbp at $z = -1$ and the complexification point at $z = 0$, giving the contour on the right.

Towards describing the leading dS_{d+1} area as well as the $O(\epsilon)$ slow-roll correction, we will find it convenient to use the variable $z = r^2 - 1$, although our analysis can be carried out in the r -variable as well (as we will describe later). The no-boundary point and the complexification point in the r - and z -variables are (Figure 3)

$$z = r^2 - 1 \quad \Rightarrow \quad (\text{nbp}) \quad r = 0 \equiv z = -1; \quad (\text{complexification}) \quad r = 1 \equiv z = 0. \quad (13)$$

The area integral is then recast as a complex contour integral: the contour C in the z -variable, with the pole $z = 0$ regulated to $z = \delta$, is

$$C = [-1, -\delta] \cup [z = \delta e^{i\theta}; \theta = \pi, \theta = 0] \cup [\delta, z_c]. \quad (14)$$

The middle leg is a semicircle of radius δ going around the pole, defined as going from $\theta = \pi$ to $\theta = 0$: then $z = \delta e^{i\pi} = -\delta$ at the left end of the semicircle (on the side of the nbp) and $z = \delta$ at its right end, around the complexification point. The details of this regulating semicircle skirting the pole at $r = 1$ or $z = 0$ are not important. In essence, we are evaluating two separate area contributions, from the Lorentzian and hemisphere regions, with regularization at the complexification point.

3.1 dS_4 area including $O(\epsilon)$ correction

We will now study the no-boundary extremal surface area (11) in 4-dim slow roll inflation: the basic setup here appears in App. A.1. The metric is of the form (7), (8), with $d = 3$, and the overall picture is as depicted in Figure 2.

The slow-roll equations of motion (50) in the slow-roll approximation become (51), *i.e.*

$$3H^2 \sim V(\phi), \quad 3H\dot{\phi} \sim -V'(\phi). \quad (15)$$

The metric component g_{aa} can be shown to take the form (see App. D)

$$g_{aa} = \frac{3 - \frac{1}{2}(a \partial_a \phi)^2}{3 - V(\phi) a^2}. \quad (16)$$

Expanding to $O(\epsilon)$ in the slow-roll correction with $\phi = \phi_* + \varphi(\tau)$ and $V(\phi) = V_* + V_*' \varphi(\tau)$, we solve the inflaton equation of motion (53) for the perturbation, imposing regularity at the no-boundary point and matching with the late time expansion (as described in [49]). This finally gives the 4-dim slow-roll inflaton profile in the $r > 1$ Lorentzian region as

$$\epsilon \equiv \frac{V_*'^2}{2V_*^2}; \quad \varphi(r) = \sqrt{2\epsilon} \tilde{\varphi}(r), \quad \tilde{\varphi}(r) = \frac{1 + i\sqrt{r^2 - 1}}{r^2} - \log(1 - i\sqrt{r^2 - 1}) - \frac{i\pi}{2}, \quad (17)$$

and the metric component $g_{rr} = g_{aa} l^2$ in the form (9), where in this 4-dim case we have

$$\beta(r) = -\frac{1}{6} \left(r \frac{\partial \tilde{\varphi}}{\partial r} \right)^2 + \frac{\tilde{\varphi} r^2}{1 - r^2}. \quad (18)$$

Inputting the inflaton profile (55) with $r = \cosh \tau$ gives $\beta(r)$ in the $r > 1$ Lorentzian region,

$$\beta_{>}(r) = \frac{8 - 9r^4 + 4ir^2\sqrt{r^2 - 1} + 8i\sqrt{r^2 - 1} - 6ir^4\sqrt{r^2 - 1} + r^6(6 \log(1 - i\sqrt{r^2 - 1}) - 1 + 3i\pi)}{6r^4(r^2 - 1)}. \quad (19)$$

To continue this to the $r < 1$ hemisphere region, we note that it is adequate to replace $-i\sqrt{r^2 - 1}$ by $\sqrt{1 - r^2}$ in $\beta_>(r)$: this defines $\beta_<(r)$.

The above recasting gives the dS_4 slow-roll inflation area to $O(\epsilon)$ as

$$S = \frac{\pi l^2}{2G_4} \int_C \frac{1 + \epsilon \beta_>(r)}{2\sqrt{1 - r^2}} r dr \equiv \frac{\pi l^2}{2G_4} \int_C \frac{1 + \epsilon \beta_>(z)}{2\sqrt{-z}} dz. \quad (20)$$

For the leading pure de Sitter piece, there are no singularities and the areas can be evaluated as separate integrals in the Lorentzian and Euclidean regions, as in (4). However for the $O(\epsilon)$ contribution to the area, it turns out that there are extra pole pieces at the complexification point $r = 1$ ($z = 0$). Thus it is important to define these as a contour integral in the complex time plane, defining a contour to avoid the pole at $r = 1$, as shown in Figure 3. We describe the detailed calculation in Appendix B, in both the z - and r -coordinates.

Adding up all the contributions along the full contour C keeping the leading order and $O(\epsilon)$ pieces in (20), we obtain

$$\begin{aligned} S = & \frac{\pi l^2}{2G_4} \left[1 - \sqrt{\delta} + \epsilon \left[\left(\log 4 - \frac{7}{6} + i\pi \right) - \left(-\frac{2 - 3i\pi}{6\sqrt{\delta}} + \frac{5}{3} \right) \right] \right. \\ & + \sqrt{\delta}(-i + 1) + \epsilon \left[\frac{2 - 3i\pi}{6i\sqrt{\delta}} - \frac{2 - 3i\pi}{6\sqrt{\delta}} \right] \\ & \left. + \frac{1}{i}(\sqrt{z_c} - \sqrt{\delta}) + \epsilon \left[\left(1 + i\frac{7}{6}\sqrt{z_c} - i\sqrt{z_c} \log \sqrt{z_c} \right) - \left(\frac{2 - 3i\pi}{6i\sqrt{\delta}} + \frac{5}{3} \right) \right] \right]. \quad (21) \end{aligned}$$

Finally, note that although we have expressed the area as a single complex-time-plane integral, we have evaluated it as separate integrals in the top timelike part and the hemisphere part, with the semicircle contour only serving to avoid the $r = 1$ ($z = 0$) pole. Note that all the singular pieces near the pole cancel as they should, so the details of the contour around the pole are unimportant. We obtain finally

$$S_{sr_4} = \frac{\pi l^2}{2G_4} \left(-i\frac{R_c}{l} + 1 \right) + \epsilon \frac{\pi l^2}{2G_4} \left(-i\frac{R_c}{l} \log \frac{R_c}{l} + i\frac{7}{6}\frac{R_c}{l} + \log 4 - \frac{7}{2} + i\pi \right), \quad (22)$$

to $O(\epsilon)$ in the slow-roll corrections. Note that the various finite pieces conspire to give the finite value above: the real part of this finite value is negative.

Unlike in the pure de Sitter case, where there was a clean separation between the real part of the area arising from the hemisphere and the imaginary part from the top timelike Lorentzian region, the slow-roll corrections contain real and imaginary parts from both the timelike and hemisphere regions. The finite terms in $S_{sr_4}^\epsilon$ in particular arise from the entire surface, both timelike and hemisphere parts.

Recalling the comments after (11), (12), the minimal time contour (Figure 3) we have employed is natural given that the slow-roll case is near de Sitter: it faithfully dovetails

with the geometric picture of time in the semiclassical near dS regime here, and encodes the shape (Figure 2) of the slow-roll IR extremal surface which is expected to be near that in pure dS (Figure 1). Dramatically changing the contour would deviate substantially from the semiclassical geometry here (also the Cauchy theorem cannot apply given the non-analytic expressions here).

It is now interesting to note that this finite value above matches precisely with the finite part in (96) of the $O(\epsilon)$ slow-roll correction in the Wavefunction of the Universe $\Psi \sim e^{iI}$ in slow-roll inflation, given in [49]: we review the details of this calculation in App. D. But to summarize, the on-shell dS_4 action with $O(\epsilon)$ slow-roll correction is

$$iI_{sr4} = \frac{\pi l^2}{2G_4} \left[1 + \epsilon \left(\log 4 - \frac{7}{2} + i\pi \right) - i \left(r_c^3 - \frac{3}{2} r_c \right) + i\epsilon \left(r_c^3 \left(\log r_c - \frac{1}{6} \right) + \frac{r_c}{4} (6 \log r_c - 11) \right) \right], \quad (23)$$

where $r_c \equiv \frac{R_c}{l}$ is the cutoff near the future boundary. The first line is mostly real while the second line is pure imaginary. We note that $|\Psi|^2 \sim e^{\frac{\pi l^2}{G_4}(1+\epsilon\#)}$ is controlled by the the real terms in the first line and is the probability for creation of this universe with slow-roll corrections. The imaginary terms cannot agree since the area corresponds to a codim-2 extremal surface with corresponding divergences while the action corresponds to the full 4-dim space with its corresponding divergences near the future boundary.

The fact that the real terms in S_{sr4} in (22) match those in iI_{sr4} in (23) is consistent with and corroborates the heuristic Lewkowycz-Maldacena interpretation in [25] of these no-boundary extremal surface areas as the amplitude for codim-2 cosmic brane creation (reviewed briefly after Figure 1). More specifically the probability for this maximal cosmic brane creation matches that for the creation of the Universe. This probability must be finite since it is ultimately dictated by the upper bound set by de Sitter entropy (the maximal amount of “stuff” in this space, controlled by the no-boundary maximal hemisphere): thus the divergent terms near the future boundary cannot contribute and must be pure imaginary. With the slow-roll corrections included, we have seen that the finite terms arise from everywhere. Note that since $\log 4 - \frac{7}{2} < 0$, the no-boundary area or the cosmic brane creation probability has decreased. This is perhaps a reflection of the fact that excitations in de Sitter space decrease its entropy (as for a black hole in de Sitter space).

It is interesting to ask what the analog in AdS is of this matching of the real finite part of the areas and the entropy contribution in the Wavefunction. The AdS Ryu-Takayanagi formulation relies on the existence of a nice optimization: minimal surfaces start at the boundary and turn around in the interior. With regard to the current context, we recall

that the RT surface on a constant time slice in the AdS black hole/brane wraps the horizon as the boundary subregion becomes the whole space, *i.e.* the maximal (IR) subregion. The finite part of the area then becomes the bulk entropy (which for the AdS black brane is the thermal entropy in the dual field theory). This entropy can also be realized by the well-known Gibbons-Hawking procedure of regarding the on-shell action as a partition function [58] and evaluating the corresponding entropy: it usefully captures phenomena in AdS/CFT such as the Hawking-Page transition [59, 60]. In the de Sitter case, there are no turning points in the Lorentzian region as we have reviewed: no-boundary extremal surfaces turn around only in the Euclidean hemisphere and give half dS entropy as the real finite part. This entropy can also be realized from the on-shell action regarded as a partition function: with the slow-roll corrections we obtain the above. The fact that the maximal cosmic brane probability matches the probability from the Wavefunction then corroborates the Lewkowycz-Maldacena arguments in [25].

It is worth noting that the divergent terms in the area (22) in the slow-roll corrections exhibit a logarithmic enhancement scaling as $R_c \log R_c$, which might seem surprising considering that the metric component g_{aa} itself (9) has only subleading pieces near the future boundary. However we note that the slow-roll correction $\beta_{>}(r)$ (19) part in g_{aa} does have a term scaling as $\log r$ for large r : thus the Lorentzian part of the area (11) of this codim-2 surface (which has extra r -factors) for large r scales as $\epsilon \log r$ which leads to the log-enhancement. Similar features appear also in the action (23) where the slow-roll correction scales as $\epsilon r_c^3 \log r_c$ while the leading term scales as $V_{S^3} \sim r_c^3$ (as noted in [49]).

(A related point is whether the logarithmic term renders the finite piece ambiguous: in this regard note that rescaling the cutoff as $R_c \rightarrow \alpha R_c$ in (22) gives an extra $\epsilon \frac{\pi l^2}{2G_4} (-i \frac{R_c}{l} \alpha \log \alpha)$ contribution from the $R_c \log R_c$ term, which modifies only the leading area law divergence term. There is no standalone $\log R_c$ term, so the finite piece is unambiguous.)

To put this enhanced logarithmic scaling in perspective, it is worth recalling similar features in AdS/CFT , especially in the context of nonrelativistic condensed matter-like generalizations and Fermi surfaces. In particular it was noted that certain classes of hyperscaling violating Lifshitz theories exhibit novel holographic entanglement scaling [68, 69, 70]. While these are phenomenological gravitational descriptions, certain gauge-string realizations were found in [71] which precisely recover this logarithmic scaling. For instance, the AdS_5 plane wave $ds^2 = \frac{R^2}{r^2} [-2dx^+ dx^- + dx_i^2 + dr^2] + R^2 Q r^2 (dx^+)^2 + R^2 d\Omega_5^2$ is interpreted as a simple anisotropic state in the dual $\mathcal{N} = 4$ Super Yang-Mills CFT_4 with holographic energy momentum density $T_{++} \sim Q$. Under x^+ -dimensional reduction this gives $ds^2 = r^{\frac{2\theta}{d_i}} \left(-\frac{dt^2}{r^{2z}} + \frac{\sum_{i=1}^{d_i} dx_i^2 + dr^2}{r^2} \right)$ with $d_i = 2$, $\theta = 1$, $z = 3$ (and $x^- \equiv t$). Holographic entanglement entropy [72] (see also [73]) for a strip subregion along the flux direction then gives the

leading divergence $S^{div} \sim N^2 \frac{V_2}{\epsilon^2}$, and the finite part $S^{fin} \sim N^2 V_2 \sqrt{Q} \log(lQ^{1/4})$. Identifying the energy flux Q and the UV cutoff ϵ with the Fermi momentum $k_F \equiv Q^{1/4} \sim \frac{1}{\epsilon}$ recasts the area law divergence as $S^{div} \sim N^2 V_2 k_F^2$ with the finite part resembling the logarithmic enhancement for a Fermi surface $S^{fin} \sim N^2 V_2 k_F^2 \log(lk_F)$. Although the *AdS/CMT* context is quite different, we see that there are structural similarities with the extremal surface areas (22). These complex areas here are expected to encode boundary entanglement entropy in the exotic Euclidean (ghost-like) CFT_3 dual to dS_4 under the slow-roll deformations sourced by the inflaton (although understanding this nontrivial dual in detail is challenging!).

Finally one might ask what the no-boundary slow-roll corrected areas map to in *AdS* under the analytic continuation $L \rightarrow -il$ which for the maximal subregions in $AdS \leftrightarrow dS$ are given by (4), (5), (6). Then the leading term in the area (22) is simply the *AdS* area in (5), but the analytic continuation of the slow-roll correction gives imaginary components as well. This suggests that the corresponding perturbations in *AdS* induce timelike components to the extremal surface. However this blithe continuation needs to be examined more carefully requiring physically reasonable scalar perturbations in *AdS* that might be analogous to the inflationary no-boundary de Sitter perturbations here.

4 Other cosmologies

We will now describe no-boundary extremal surfaces in some other cosmological spacetime backgrounds, including in particular dS_3 slow-roll inflation, and Schwarzschild de Sitter black holes with small mass.

4.1 dS_3 area including $O(\epsilon)$ correction

We can generalize the above 4-dim analysis in sec. 3.1 to 3-dimensions and study 3-dim slow roll inflation: the basic setup here appears in App. A.2. The 3-dim gravity case has no intrinsic dynamics but the inflaton scalar degree of freedom makes it more interesting, even if this is just a toy model of slow-roll inflation. The metric is of the form (7), (8), with $d = 2$, and the overall picture is as depicted in Figure 2.

Here we have the slow-roll equations of motion (58), which in the slow-roll approximation become (59), *i.e.*

$$H^2 \sim V(\phi), \quad 2H\dot{\phi} \sim -V'(\phi). \quad (24)$$

The inflaton equation of motion (60) for the perturbation can be solved as in the dS_4 slow-roll case, imposing regularity at the no-boundary point and matching with the late time

expansion. This finally gives the solution as (63), *i.e.*

$$\varphi(\tau) = \sqrt{2\epsilon} \left[\left(\frac{i\pi}{4} - \frac{\tau}{2} \right) \tanh \tau + \frac{\log 2}{2} - \frac{i\pi}{4} \right] \equiv \sqrt{2\epsilon} \tilde{\varphi}(\tau). \quad (25)$$

The slow-roll correction to the metric here, using $r = \cosh \tau$, is

$$g_{rr} = \frac{1 - \frac{1}{2}(r\partial_r\varphi)^2}{1 - Vr^2} \simeq \frac{1}{1 - r^2} (1 + 2\epsilon\beta_>(r)) \quad (26)$$

where

$$2\epsilon\beta_>(r) \equiv \frac{V'^2}{V_*^2} \left(-\frac{1}{2}(r\partial_r\tilde{\varphi})^2 + \frac{\tilde{\varphi}^2 r^2}{1 - r^2} \right) \quad (27)$$

evaluates to the expression in (76).

The slow-roll dS_3 inflation no-boundary extremal surface area in (12) is

$$S_{sr3} \simeq \frac{l}{2G_3} \left(\int_{\delta}^{z_c} \frac{1 + \epsilon\beta_>(z)}{2i\sqrt{z(1+z)}} dz + \int_{\delta}^1 \frac{1 + \epsilon\beta_<(z)}{2\sqrt{z(1-z)}} dz \right) + \frac{l}{2G_3} I_{\epsilon}^{\theta} \quad (28)$$

where I_{ϵ}^{θ} is the contribution from the semicircle part of the contour, skirting around the pole at $z = 0$. We have written this in terms of the variable $z = r^2 - 1$ in (13) for $z > 0$ and then continued as $z \rightarrow -z$ to the hemisphere region, as in the dS_4 case.

We describe the details of this calculation in Appendix C. From there, we obtain

$$\begin{aligned} S = & \frac{l}{2G_3} \left[\frac{\pi}{2} + \epsilon \left[\frac{1}{16} i \left(-(\log z_c)^2 + \log z_c + \pi^2 + 4i\pi + 4(\log 2)^2 - 6 \log 2 \right) \right. \right. \\ & \left. \left. - \left(-\frac{\pi}{8} + \frac{i(8i\pi + \pi^2 - 4 \log(16))}{32\sqrt{\delta}} \right) \right] \right] + I_{\epsilon}^{\theta} \\ & \left. - i \log \sqrt{z_c} + \epsilon \left[\frac{\pi}{16} (2\pi i - 1 - \log 16) - \left(-\frac{\pi}{8} + \frac{(8i\pi + \pi^2 - 4 \log(16))}{32\sqrt{\delta}} \right) \right] \right] \end{aligned} \quad (29)$$

which simplifies to (after rewriting using $z = r^2 - 1$ and expanding at large $r_c = \frac{R_c}{l}$)

$$\begin{aligned} S = & \frac{l}{2G_3} \left(\frac{\pi}{2} - i \log \frac{R_c}{l} \right) \\ & + \epsilon \frac{l}{2G_3} \left(-\frac{\pi}{16} (1 + \log 16) + \frac{i}{16} \left(2 \log \frac{R_c}{l} - 4 \left(\log \frac{R_c}{l} \right)^2 + 3\pi^2 + 4(\log 2)^2 - 6 \log 2 \right) \right). \end{aligned} \quad (30)$$

The real part of the area including the slow-roll correction here is

$$\text{Re}S = \frac{\pi l}{4G_3} - \epsilon \frac{l}{2G_3} \frac{\pi}{16} (1 + \log 16). \quad (31)$$

As in dS_4 inflation, this in fact matches the real parts in (99) and (101) in App. D obtained to $O(\epsilon)$ from the semiclassical expansion of action or the the logarithm of the Wavefunction, *i.e.* $\log \Psi \sim iI_{cl}$. Thus the maximal cosmic brane creation probability matches the probability $|\Psi|^2$ for Universe creation, corroborating the heuristic Lewkowycz-Maldacena interpretation in [25] of these no-boundary extremal surface areas.

The details of this calculation appear in App. D. The imaginary finite pieces in (99), (101) do not agree. The dual here is an even-dimensional CFT and anomaly contributions of the CFT on a 2-sphere are expected to give further pure imaginary contributions. The CFT anomaly is expected to be proportional to the central charge which in dS_3/CFT_2 is pure imaginary. It would be interesting to understand this breaking of dual conformal invariance by such inflationary perturbations in greater detail.

In this light, it is worth looking more closely at the leading term as well. This in fact contains a subleading finite term near the future boundary: we have the timelike part of the area $-i\frac{l}{2G_3} \int_1^{R_c/l} \frac{dr}{\sqrt{r^2-1}} = -i\frac{l}{2G_3} \log \frac{R_c}{l} - i\frac{l}{2G_3} \log 2$, noting that the indefinite integral is $\log(r + \sqrt{r^2-1})$. This subleading finite term is pure imaginary so the real part of the area controlling the cosmic brane creation probability remains half dS_3 entropy.

4.2 Schwarzschild de Sitter black holes with small mass

We will discuss Schwarzschild de Sitter black holes here, but with the black hole mass treated as perturbation: some useful references include [50, 51], as well as our previous work [74, 75, 76]. The metric is

$$ds^2 = -f(r)dt^2 + \frac{dr^2}{f(r)} + r^2 d\Omega_2^2, \quad f(r) = 1 - \frac{2m}{r} - \frac{r^2}{l^2}. \quad (32)$$

The metric function can be written as

$$f(r) = \frac{1}{l^2 r} (r_D - r)(r_D + r_S + r)(r - r_S), \quad r_D r_S (r_D + r_S) = 2ml^2, \quad r_D^2 + r_D r_S + r_S^2 = l^2. \quad (33)$$

The roots r_S and r_D correspond to the black hole and cosmological horizons respectively, and satisfy the constraint relations above, alongwith $0 \leq r_S \leq r_D \leq l$. In addition, we have the condition $\frac{m}{l} \leq \frac{1}{3\sqrt{3}}$ for a physical black hole horizon to exist.

In the limit of small mass $m \ll l$, the roots representing the horizon locations can be approximated as

$$r_D \sim l - G_4 m, \quad r_S \sim 2G_4 m, \quad (34)$$

so that the cosmological horizon at $r_D = l$ shifts a little inward for a nonzero black hole horizon. Since there is a curvature singularity at $r = 0$ inside the black hole horizon, strictly

speaking there is no smooth Euclidean instanton that can be extended to a smooth no-boundary geometry. However treating the black hole perturbation to only serve to shift the cosmological horizon, we can look for a no-boundary geometry continuing to take the no-boundary point as $r = 0$. In other words, we disregard the spacetime geometry effects of the black hole (and thus disregard the singularity etc). This amounts to approximating the metric function as

$$f(r) = \frac{1}{l^2} (r_D^2 - r^2 + r_S(r_D - r)) \left(1 - \frac{r_S}{r}\right) \xrightarrow{r_S \rightarrow 0, l \sim r_D} 1 - \frac{r^2}{r_D^2}. \quad (35)$$

Now we Euclideanize $t = i\tau_E$, and for $r < r_D$ we glue on a Euclidean hemisphere which is smooth at the no-boundary point $r = 0$, and thus replaces the earlier SdS geometry.

On the $t = \text{const}$ slice taken as a boundary Euclidean time slice, we consider the maximal (hemisphere) subregion on the S^2 at the future boundary. Then the no-boundary area becomes

$$S = \frac{V_{S^1}}{4G_4} \int_0^{r_D} \frac{r dr}{\sqrt{1 - \frac{r^2}{r_D^2}}} + \frac{(-i)V_{S^1}}{4G_4} \int_{r_D}^{R_c} \frac{r dr}{\sqrt{\frac{r^2}{r_D^2} - 1}}. \quad (36)$$

This gives

$$S = -i \frac{\pi r_D^2}{2G_4} \frac{R_c}{r_D} + \frac{\pi r_D^2}{2G_4}. \quad (37)$$

The real part of this area is half the entropy of the shifted cosmological horizon with size $r_D \sim l - G_4 m$: in other words, treating this as just a modified no-boundary de Sitter space, we obtain the earlier result for pure dS_4 . To $O(m)$, this gives

$$\text{Re}S \sim \frac{\pi}{2G_4} (l - G_4 m)^2 \sim \frac{\pi l^2}{2G_4} - \pi l m, \quad (38)$$

This matches half the Euclidean action, expanded to $O(m)$, for Schwarzschild de Sitter black holes obtained in [77] by a careful treatment of the conical singularities at the two horizons incorporating δ -function sources there. However it is worth emphasizing that the extremal surface area has been obtained under the approximation (35). It would be worth refining this more carefully.

For 3-dim Schwarzschild de Sitter given by

$$ds^2 = -f(r)dt^2 + \frac{dr^2}{f(r)} + r^2 d\phi^2, \quad f(r) = 1 - 8G_3 E - \frac{r^2}{l^2}. \quad (39)$$

In this case, there is only one horizon at $r_D = l\sqrt{1 - 8G_3 E}$. At sufficiently large E , the space closes up and the entropy $\frac{\pi r_D}{2G_3}$ vanishes. As before, for small energy E , we approximate the metric function as $f(r) \sim 1 - \frac{r^2}{r_D^2}$ and evaluate the hemisphere contribution to the no-boundary area as

$$S^h = \frac{2}{4G_3} \int_0^{r_D} \frac{dr}{\sqrt{1 - \frac{r^2}{r_D^2}}} = \frac{\pi r_D}{4G_3}, \quad (40)$$

which is half the entropy of the modified dS_3 space (compare (1)). However it is worth noting that the area calculation done exactly instead gives

$$S^{th} = \frac{2}{4G_3} \int_0^{r_D} \frac{dr}{\sqrt{1 - 8G_3 E - \frac{r^2}{l^2}}} = \frac{\pi l}{4G_3}, \quad (41)$$

which is half dS_3 entropy independent of the mass E . It is important to note however that in this case, the location $r = 0$ is a conical singularity as can be seen from the metric there, *i.e.* $ds^2 \sim -\frac{r_D^2}{l^2} dt^2 + \frac{l^2 dr^2}{r_D^2} + r^2 d\phi^2 \sim -dt'^2 + dr'^2 + r'^2 d\phi'^2$ redefining $t' = \frac{r_D}{l} t$, $r' = \frac{lr}{r_D}$, $\phi' = \frac{r_D}{l} \phi$ (see *e.g.* [12]). Thus we see that for $r_D < l$, the angle ϕ' is identified modulo $2\pi \frac{r_D}{l}$ reflecting the conical singularity at $r = 0$. Thus the area S^{th} pertains to this singular space while S^h pertains to the no-boundary space obtained from SdS_3 under the approximations of $f(r)$.

Thus overall, it is important to note that Schwarzschild de Sitter spaces for generic mass have distinct Euclidean periodicities at the black hole and cosmological horizons so they cannot be made regular except at the extremal Nariai point. Thus in evaluating these no-boundary extremal surface areas we are making approximations to construct appropriate no-boundary geometries for small mass perturbations near de Sitter. Perhaps one may better define these areas by more careful treatment of the conical singularities for generic mass.

4.2.1 Extremal SdS_4 : Nariai

The Nariai or extremal limit of Schwarzschild de Sitter gives a near horizon $dS_2 \times S^2$ geometry. This occurs when $r_D = r_S$: then (33) gives $r_D = r_S = r_0 = \frac{l}{\sqrt{3}}$ and $\frac{m}{l} = \frac{1}{3\sqrt{3}}$. This is a degenerate limit but regulating near Nariai as $r_D = r_0 - x$, $r_S = r_0 + x$, gives

$$f(r) \sim \frac{3}{l^2} (x^2 - (r - r_0)^2), \quad (42)$$

where we approximate $r \sim r_0$ in the $(r_D + r_S + r)$ factor. This amounts to zooming in to the extremal throat region, with the transverse S^2 of size $r_0 = \frac{l}{\sqrt{3}}$. Defining

$$\psi = \int \frac{dr}{\sqrt{f(r)}} = \frac{l}{\sqrt{3}} \sin^{-1} \frac{r - r_0}{x} \equiv \frac{l}{\sqrt{3}} \tilde{\psi}, \quad (43)$$

the metric on the $t = \text{const}$ slice approximates to

$$ds^2 \sim d\psi^2 + \frac{l^2}{3} d\Omega_2^2. \quad (44)$$

For the no-boundary hemisphere we have $\tilde{\psi} \in [0, \frac{\pi}{2}]$, so the area for a hemispherical cap on an equatorial plane in the S^2 is approximated as

$$S \sim \frac{l^2}{3} \int_0^{\frac{\pi}{2}} d\tilde{\psi} \frac{V_{S^1}}{4G_4} = \frac{\pi}{6} \frac{\pi l^2}{2G_4}, \quad (45)$$

which is a factor $\frac{\pi}{6} \sim \frac{1}{2}$ times dS_4 entropy. On the other hand, the Euclidean action for the Nariai limit $dS_2 \times S^2$ is a factor $\frac{2}{3}$ times that for dS_4 [50, 51]. This mismatch is perhaps not surprising since the Nariai limit is far from pure de Sitter, unlike the previous cases we have discussed.

4.3 FRW+slow-roll cosmologies

Generic FRW-type cosmologies with spatial S^d slices are of the form

$$ds^2 = -dt^2 + a^2(t)d\Omega_d^2, \quad a(t) \sim t^\nu. \quad (46)$$

From the point of view of the slow-roll inflation phase evolving to an FRW cosmology epoch (schematically as in Figure 2), we are interested only in regarding this as a Lorentzian FRW space with the timelike part of the slow-roll inflation extremal surfaces joining at the reheating surface (approximately the future boundary) with timelike extremal surfaces in the FRW phase. We restrict to a boundary Euclidean time slice as some S^d equatorial plane and pick maximal (hemisphere) subregions. Then the Lorentzian FRW region gives timelike extremal surfaces with area (suppressing intrinsic FRW lengthscales)

$$S_{FRW} = -i \frac{V_{S^{d-2}}}{4G_{d+1}} \int_{t_0}^{t_l} dt a(t)^{d-2} \xrightarrow{4-dim} -i \frac{\pi}{2G_4} (t_l^{\nu+1} - t_0^{\nu+1}). \quad (47)$$

Appending (22), the full extremal surface area for the FRW+inflation cosmology becomes $S_{FRW} + S_{sr4}$. It may be interesting to understand if these sorts of codim-2 area observables can be usefully employed to understand aspects of cosmological observations.

Considering the FRW spaces (46) in themselves, in general these will not admit any smooth HH no-boundary Euclidean continuation. Blithely calculating the IR no-boundary extremal surface area gives the Euclidean hemisphere contribution as

$$\begin{aligned} S &= \frac{V_{S^{d-2}}}{4G_{d+1}} \int_0^{\tau_l} d\tau_E a(\tau_E)^{d-2} = \frac{V_{S^{d-2}}}{4G_{d+1}} \int_0^{\tau_l} \frac{da a(\tau_E)^{d-2}}{(da/d\tau_E)} \\ &\sim \frac{V_{S^{d-2}}}{4G_{d+1}} \int_0^{\tau_l} d\tau_E \tau_E^{(d-2)\nu} \xrightarrow{4-dim} \frac{\pi}{2G_4} \frac{\tau_l^{\nu+1}}{\nu+1}. \end{aligned} \quad (48)$$

where we have taken $a(\tau_E) \sim \tau_E^\nu$, with $\nu > 0$. The sphere S^d shrinks to zero size at the no-boundary point $\tau_E = 0$: however for generic ν , the derivative $\frac{da}{d\tau_E}$ is not smooth so a Big-Bang type singularity persists at $\tau_E = 0$.

5 Discussion

Building on previous work on de Sitter extremal surfaces anchored at the future boundary, we have studied no-boundary extremal surfaces in slow-roll inflation models, with perturbations

to no-boundary global dS preserving the spatial isometry. In pure de Sitter space (Figure 1) the Euclidean hemisphere gives a real area equalling half de Sitter entropy [23], [24], while the timelike surfaces from the top Lorentzian part give pure imaginary area (see (4), (5), (6)). There is thus a clean separation between the real and imaginary parts of these areas which are best interpreted as time-entanglement or pseudo-entropy. A heuristic Lewkowycz-Maldacena argument [25] executing the replica argument on $Z_{CFT} = \Psi_{dS}$ for maximal no-boundary surfaces corroborates this interpretation since this is now a replica on the Wavefunction regarded as an amplitude. In the slow-roll case, we employ the explicit analytic expressions described in [49] for the slow-roll metric perturbations. The presence of these perturbations (small wiggles around dS , Figure 2) mixes up everything so the no-boundary extremal surface areas here have nontrivial real and imaginary pieces overall. We evaluate the area integrals in the complex time-plane defining appropriate contours designed to avoid extra poles that arise at the complexification point due to the perturbations (similar features arise in the evaluation of the Wavefunction of the Universe). For the 4-dimensional slow-roll inflation case, the real and imaginary finite corrections (22) at leading order in the slow-roll parameter match those in the semiclassical expansion of the Wavefunction (or action). In 3-dimensional inflation, we find that the real finite parts of the area (30) agree with those in the Wavefunction (action): the imaginary finite parts do not agree, perhaps reflecting the dual CFT on an even dimensional sphere (with potential anomalies controlled by the imaginary central charge in dS_3/CFT_2). Overall the maximal cosmic brane creation probability controlled by the real parts of the no-boundary extremal surface areas match the probability from the semiclassical Wavefunction, corroborating the cosmic brane interpretation in [25]. The matching of these maximal probabilities is perhaps expected since this is the maximal amount of “stuff” in the space (in general dual conformal invariance is broken but small corrections of the kind here do not wreck this maximal probability). The slow-roll corrections decrease this maximal probability (equal to half de Sitter entropy for pure dS), perhaps reflecting the fact that small excitations in dS decrease the entropy. We have also studied no-boundary extremal surfaces in Schwarzschild de Sitter spaces with small mass, with various overall similarities, as well as other generic cosmologies.

Stepping back and looking at a broad-brush level, it is important to understand the connections between the no-boundary extremal surface areas and the Wavefunction of the Universe in greater detail (mirroring connections between boundary entanglement entropy and Z_{CFT} in the exotic duals here): among other things this will shed light on the underlying structure of these extremal surface areas in dS and cosmology more broadly. There is a rich history of such studies in AdS/CFT on extremal surface areas and the bulk partition function (dual to entanglement entropy and the boundary partition function) [4, 5, 6, 7]. One such

fact is that for maximal (IR) subregions in the AdS black hole/brane, the RT minimal surface dips all the way into the interior and wraps the horizon so the finite part of entanglement entropy is the black hole/brane entropy. This entropy can also be realized from the action regarded as a partition function. In the current context, a similar observation is that the real finite part of the no-boundary extremal surface in pure de Sitter is half dS entropy, which also arises from the real part of the Wavefunction. It is natural to ask if this correlation [25] between the cosmic brane creation probability (encoded by the real finite parts of the areas) and $|\Psi_{dS}|^2$ continues away from de Sitter. An interesting class of near dS spaces comprises slow-roll inflation. Our studies vindicate this correlation here.

As we have seen, we have found it necessary to define the area integrals in the complex-time plane with appropriate contours required to avoid extra poles at the complexification point. We have done this in the minimal way, by simply evaluating the areas as separate integrals in the Lorentzian and hemisphere regions, with the regulating time contour Figure 3 serving to simply remove the poles (and the details of the regularization are unimportant). The integrals involve non-analytic expressions so one might expect that changing the contour dramatically is not a reasonable thing to do in these complex-valued integrals (and the Cauchy theorem cannot apply). This can be corroborated further in the present case noting that since the slow-roll case is near de Sitter we expect on physical/geometric grounds that the time contour should also be near that in de Sitter. In de Sitter the time contour encodes the IR extremal surface shape in Figure 1 so it is natural that the time contour in the slow-roll case encodes the wiggly shape for the IR extremal surface in Figure 2: this justifies the minimal time contour Figure 3 that we have employed as quite reasonable and natural here. Roughly the time contour dovetails with the geometric picture of time in the semiclassical regimes we have here, near pure de Sitter: indeed any time contour with large deviation from the semiclassical geometry would perhaps be unphysical for the present purposes. In general, these sorts of cosmological perturbations lead to complex metrics that must be treated carefully (the complex nature is not surprising since the no-boundary condition [48] is a regularity condition analogous to positive frequency not reality; see comments in [49] as well as [10]). Thus along the lines of the analysis here, it would be interesting to understand if these sorts of no-boundary extremal surface areas can be evaluated meaningfully and unambiguously for complex metrics appearing in cosmology more generally, and whether they give insights into complex metrics and the KSW criterion [78, 79] (see also [57]).

The classes of de Sitter perturbations we have studied here all preserve the spherical isometry of the S^3 slices in global dS_4 . Thus all boundary Euclidean time equatorial plane slices are equivalent, with the corresponding codim-2 no-boundary extremal surface areas all equal. For more general inflationary perturbations with inhomogeneities in particular, we

expect that different boundary Euclidean time slices are inequivalent and thus will lead to inequivalent codim-2 extremal surfaces anchored at the future boundary (an example of this inequivalence was already noted in [20], [24] for the extremal surface areas in different slices of dS in the static coordinatization). It would be interesting to explore this further.

The extremal surfaces discussed here and in earlier work have been studied directly and via analytic continuations from AdS but they are the analogs in some sense of the AdS RT minimal surfaces on constant time slices (which map to the boundary Euclidean time slices stretching from the future boundary here). In that light, it is natural to ask for covariant (HRT-like) formulations of these extremal surfaces and the corresponding areas as pseudo-entropy. One might imagine that the corresponding complex-time-plane contour analogs of Figure 3 might then be expressed more covariantly.

Finally it would be interesting to understand the analyses here from the point of view of the dual field theory. In a broad sense, dS/CFT [8, 9, 10] is a way to organize de Sitter perturbations in the language of AdS/CFT (and analytic continuations) especially as formulated in [10], and in more recent studies *e.g.* [80, 81, 82]. In this light, it would be interesting to understand the structure of inflationary perturbations and the way they reflect in the no-boundary extremal surface areas regarded as pseudo-entropy. Hopefully quantum information ideas and techniques along these lines will help shed further light on de Sitter holography and the emergence of time.

Acknowledgements: It is a pleasure to thank Pawel Caputa, Bartek Czech, Matt Headrick, Michal Heller, Alok Laddha, Shiraz Minwalla, Rob Myers, Suvrat Raju, Ronak Soni, Tadashi Takayanagi and Sandip Trivedi, on aspects of [24, 25], and the present studies, as well as Ronak Soni and Tadashi Takayanagi for useful comments on a draft. We thank the Organizers of the “Quantum Information, Quantum Field Theory and Gravity” Workshop, ICTS Bangalore, 2024, for hospitality while this work was nearing completion. This work is partially supported by a grant to CMI from the Infosys Foundation.

A The basic setup on inflation

A.1 dS_4 slow roll

This pertains to sec. 3.1 in the main text. We will be brief in our review of pertinent points of inflation: general useful reviews include [66, 67], and [48]-[57]. The action for the 4-dim Einstein scalar theory (with $8\pi G_N = 1$) is

$$I = \int d^4x \sqrt{g} \left(\frac{R}{2} - \frac{1}{2} (\nabla\phi)^2 - V(\phi) \right) - \int d^3x \sqrt{h} K. \quad (49)$$

With $ds^2 = -dt^2 + a(t)^2 d\Omega_3^2$, $\phi = \phi(t)$, the equations of motion become

$$\begin{aligned} 3H^2 &= 3 \left(\frac{\dot{a}}{a} \right)^2 = -\frac{3}{a^2} + \frac{1}{2} \dot{\phi}^2 + V(\phi), \\ \ddot{\phi} + 3H\dot{\phi} + V'(\phi) &= 0. \end{aligned} \quad (50)$$

In the slow roll approximation, the inflaton kinetic term is subdominant relative to the potential: for large 3-sphere size a_r near the end of inflation, we ignore the $\frac{3}{a^2}$ curvature term in (50), which then gives

$$3H^2 \sim V(\phi), \quad 3H\dot{\phi} \sim -V'(\phi). \quad (51)$$

At ‘‘horizon crossing’’ $\phi = \phi_*$, we have $H_* \equiv H(\phi_*) = \frac{1}{a_*} = \frac{1}{a_r} e^{\mathcal{N}(\phi, \phi_*)}$ and the leading dS metric is (7) with radius $H_*^{-1} = l$, and

$$l \equiv \frac{1}{H_*}, \quad H_*^2 \sim \frac{V_*}{3}, \quad \tau = H_* t. \quad (52)$$

For the inflaton perturbation, the equation of motion alongwith the slow-roll parameter ϵ gives

$$\phi = \phi_* + \varphi : \quad \partial_\tau^2 \varphi + 3 \tanh \tau \partial_\tau \varphi + 3\sqrt{2}\epsilon = 0, \quad \epsilon \equiv \frac{V_*'^2}{2V_*^2}. \quad (53)$$

Solving this with $A = \frac{V_*'}{H_*^2} = 3\sqrt{2}\epsilon$ gives

$$\varphi(\tau) = -\frac{1}{3} A \log(\cosh \tau) + \frac{1}{6} \text{sech}^2 \tau (2A + 3c_1 \sinh \tau) + c_1 \tan^{-1} \left(\tanh \frac{\tau}{2} \right) + c_2. \quad (54)$$

Imposing regularity at the no-boundary point $\tau = i\frac{\pi}{2}$ (via the φ -derivative) fixes $c_1 = -\frac{2A}{3i}$. This then gives

$$\varphi(\tau) = \frac{V_*'}{V_*} \left(\frac{1 + i \sinh \tau}{\cosh^2 \tau} - \log(1 - i \sinh \tau) - i\frac{\pi}{2} \right) = \frac{V_*'}{V_*} \tilde{\varphi}(\tau). \quad (55)$$

The constant \tilde{c}_2 (with $c_2 = \frac{V_*'}{V_*} \tilde{c}_2$ in (54)) inside the bracket has been fixed to $-i\frac{\pi}{2}$ by expanding at late times (large τ), which gives

$$\varphi(\tau) = \frac{V_*'}{V_*} \tilde{\varphi}(\tau) = \frac{V_*'}{V_*} \left[-\tau + \log 2 + i\frac{\pi}{2} + \tilde{c}_2 + \dots \right]. \quad (56)$$

This gives $\tilde{c}_2 = -i\frac{\pi}{2}$ to match with the slow roll solution expanded around ϕ_* at large τ :

$$\phi = \phi_* - \frac{V_*'}{V_*} \log \left(\frac{a}{a_*} \right) = \phi_* - \frac{V_*'}{V_*} \log \left(\frac{\cosh \tau}{H_* a_*} \right) \sim \phi_* - \frac{V_*'}{V_*} (\tau - \log 2). \quad (57)$$

Putting all this together finally gives (17). This completes our quick review, following [49].

A.2 dS_3 slow roll

The overall setup for inflation is very similar so we will simply list the central expressions used in sec. 4.1. The equations of motion (with $8\pi G = 1$) are

$$\begin{aligned} H^2 &= \left(\frac{\dot{a}}{a}\right)^2 = -\frac{1}{a^2} + \frac{1}{2}\dot{\phi}^2 + V(\phi), \\ \ddot{\phi} + 2H\dot{\phi} + V'(\phi) &= 0. \end{aligned} \quad (58)$$

In the slow roll approximation these give

$$H^2 \sim V(\phi), \quad 2H\dot{\phi} \sim -V'(\phi), \quad \rightarrow \quad H_* \equiv H(\phi_*), \quad H_*^2 \sim V_*, \quad (59)$$

with the second set of expressions obtained when the 2-sphere size crosses the horizon.

The inflaton equation (58) expanding for the perturbation as $\phi = \phi_* + \varphi$ becomes

$$\partial_\tau^2 \varphi + 2 \tanh \tau \partial_\tau \varphi + \frac{V'_*}{H_*^2} \varphi = 0. \quad (60)$$

With $\sqrt{2\epsilon} = \frac{V'_*}{H_*^2} = \frac{V'_*}{V_*}$ this has the solution

$$\varphi(\tau) = c_2 + \tanh \tau \left(c_1 - \frac{\sqrt{\epsilon} \tau}{\sqrt{2}} \right). \quad (61)$$

Regularity at $\tau = i\frac{\pi}{2}$ fixes $c_1 = i\frac{\pi\sqrt{\epsilon}}{2\sqrt{2}}$. The constant c_2 is fixed by matching with the slow roll solution expanded around ϕ_* at late times (large τ),

$$\phi = \phi_* - \frac{V'_*}{V_*} \log\left(\frac{a}{a_*}\right) = \phi_* - \frac{V'_*}{V_*} \left(\frac{\tau}{2} - \frac{\log 2}{2} \right). \quad (62)$$

This finally gives the inflaton profile as

$$\varphi(\tau) = \sqrt{2\epsilon} \left[\left(\frac{i\pi}{4} - \frac{\tau}{2} \right) \tanh \tau + \left(\frac{\log 2}{2} - \frac{i\pi}{4} \right) \right]. \quad (63)$$

B Details: dS_4 slow-roll area

We describe details of the calculation of the no-boundary extremal surface area for dS_4 slow roll inflation here. The leading contribution to the area (20) over the contour (Figure 3) is

$$\begin{aligned} S_0 &= \frac{\pi l^2}{2G_4} \left(\int_{y=1}^{y=\delta} \frac{d(-y)}{2\sqrt{y}} + \int_{\theta=\pi}^{\theta=0} \frac{d(\delta e^{i\theta})}{2\sqrt{-\delta} e^{i\theta}} + \frac{1}{i} \int_{\delta}^{z_c} \frac{dz}{2\sqrt{z}} \right) \\ &= \frac{\pi l^2}{2G_4} \left(-\sqrt{-z} \Big|_{-1}^{-\delta} + \sqrt{\delta} (-\sqrt{-e^{i\theta}}) \Big|_{\theta=\pi}^{\theta=0} + \frac{1}{i} \sqrt{z} \Big|_{\delta}^{z_c} \right) \\ &= \frac{\pi l^2}{2G_4} \left(1 - \sqrt{\delta} + \sqrt{\delta}(-i + 1) + \frac{1}{i}(\sqrt{z_c} - \sqrt{\delta}) \right). \end{aligned} \quad (64)$$

On the $[-1, 0]$ leg we have redefined $z = -y$ which makes this piece $\int_{\delta}^1 \frac{dy}{2\sqrt{y}}$. On the semicircle we have $z = \delta e^{i\theta}$ as stated above and we then integrate in terms of the variable $e^{i\theta}$. Of course here there is no singularity at $z = 0$ but we have written this explicitly above to normalize this calculation with the slow-roll correction to follow. So we obtain simply (with $z_c \sim R_c^2$) $S = \frac{\pi l^2}{2G_4}(1 - i\frac{R_c}{l})$, after reinstating the dimensionful dS_4 scale l .

To calculate the $O(\epsilon)$ slow-roll correction, we first note that the correction to the metric component g_{rr} in (19) is recast in the z -variable in (13) for $z > 0$ (*i.e.* the Lorentzian region $r > 1$) as

$$\beta_{>}(z) = \frac{i \left(3\pi(z+1)^3 + (z^{3/2} + 9iz - 12\sqrt{z} - 2i)(-1 - i\sqrt{z})^3 \right)}{6z(z+1)^2} + \frac{(z+1) \log(1 - i\sqrt{z})}{z}, \quad (65)$$

and we obtain

$$I_{\epsilon}^{>} = \int \frac{\beta_{>}(z)}{2i\sqrt{z}} dz = \frac{1}{6i\sqrt{z}} (2 - 3i\pi(1-z) - 7z - 6(1-z) \log(1 - i\sqrt{z})) + \frac{2/3}{1 - i\sqrt{z}}, \quad (66)$$

with $z > 0$ in this expression. It turns out happily that these integrals can be evaluated in Mathematica (with some care in evaluating them as non-analytic complex objects): the integrated expression can also be cross-checked manually of course. To evaluate the slow-roll correction area integral in the hemisphere region $r < 1$, we continue to $z < 0$: in this regard note that

$$\int_{-1}^{-\delta} \frac{\beta_{>}(z)}{2\sqrt{-z}} dz = \int_1^{\delta} \frac{\beta_{>}(-y)}{2\sqrt{y}} d(-y) = \int_{\delta}^1 \frac{\beta_{<}(y)}{2\sqrt{y}} dy \equiv I_{\epsilon}^{<}(z). \quad (67)$$

Thus it is adequate to analytically continue the integrated expression $I_{\epsilon}^{>}(z)$ to the hemisphere as $z \rightarrow -z$, and we obtain the indefinite integral in the $O(\epsilon)$ piece here as

$$I_{\epsilon}^{<}(z) = I_{\epsilon}^{>}(-z) = \frac{1}{6\sqrt{z}} (-2 + 3i\pi(1+z) - 7z + 6(1+z) \log(1 + \sqrt{z})) + \frac{2/3}{1 + \sqrt{z}}, \quad (68)$$

with $z > 0$ in this expression now.

Expanding $I_{\epsilon}^{>}$ in the $z > 0$ part of the contour, we obtain

$$z = z_c \rightarrow \infty : \quad I_{\epsilon}^{>} = 1 + i\frac{7}{6}\sqrt{z_c} - i\sqrt{z_c} \log \sqrt{z_c}; \quad z = \delta : \quad I_{\epsilon}^{>} = \frac{2 - 3i\pi}{6i\sqrt{\delta}} + \frac{5}{3}, \quad (69)$$

and we have regulated $z = 0^+$ by $z = \delta > 0$. In obtaining the above, we have expanded $\log(1+z) \sim z$ for small z in the various expressions, and used $\log(-1) = i\pi$, $\log(\pm i) = \pm \frac{i\pi}{2}$. This is important in order to cancel real divergent terms for large z_c : as it stands we see that all the divergent terms for large z_c are pure imaginary.

Expanding $I_{\epsilon}^{<}$ in the $z < 0$ part of the contour, we obtain near $z = 1$ (nbp) and $z = \delta$ (which is near 0^- in the earlier variable)

$$z = 1 : \quad I_{\epsilon}^{<} = \frac{1}{6}(-2 + 6i\pi - 7 + 12 \log 2) + \frac{1}{3}, \quad z = \delta : \quad I_{\epsilon}^{<} = \frac{-2 + 3i\pi}{6\sqrt{\delta}} + \frac{5}{3}. \quad (70)$$

Along the regulating semicircle around $z = 0$ with small $z = \delta$, examining the asymptotics of $I_\epsilon^>$, we obtain

$$I_\epsilon^\theta \Big|_{\theta=\pi}^{\theta=0} = \left(\frac{2 - 3i\pi}{6\sqrt{-\delta}e^{i\theta}} \right) \Big|_{\theta=\pi}^{\theta=0} = \frac{2 - 3i\pi}{6i\sqrt{\delta}} - \frac{2 - 3i\pi}{6\sqrt{\delta}}. \quad (71)$$

Note that near $z = 0$, we have $\beta_>(z) = -\frac{2-3i\pi}{6z}$ as the leading singular behaviour. Integrating this around the semicircle explicitly recovers the above.

Adding up all the above contributions to the area (20) finally gives (21).

One may question whether the above calculation in the z -variable has introduced subtleties due to the $\sqrt{-z}$ in various places. It turns out that the area can also be calculated directly in the form (11) in the r -coordinate (*e.g.* by evaluating in Mathematica). Using $\beta_>(r)$ in (19), we obtain below the indefinite integrals $I^>(r)$ and $I^<(r)$ respectively:

$$-i \int \frac{1 + \epsilon \beta_>(r)}{\sqrt{r^2 - 1}} r dr = -i\sqrt{r^2 - 1} - i\epsilon \frac{1}{6r^2\sqrt{r^2 - 1}} \left[\left(3i\pi r^4 - 7r^4 - 6i\pi r^2 + 5r^2 \right. \right. \\ \left. \left. + 4(1 + i\sqrt{r^2 - 1}) + 6r^2(r^2 - 2) \log(1 - i\sqrt{r^2 - 1}) \right) \right]. \quad (72)$$

$$\int \frac{1 + \epsilon \beta_<(r)}{\sqrt{1 - r^2}} r dr = -\sqrt{1 - r^2} + \epsilon \frac{1}{6r^2\sqrt{1 - r^2}} \left[\left(3i\pi r^4 - 7r^4 - 6i\pi r^2 + 5r^2 \right. \right. \\ \left. \left. + 4(1 - \sqrt{1 - r^2}) + 6r^2(r^2 - 2) \log(1 + \sqrt{1 - r^2}) \right) \right]. \quad (73)$$

In the second integral ($r < 1$) above, we have obtained $\beta_<(r)$ by continuing $\beta_>(r)$ to $r < 1$, which amounts to simply replacing $-i\sqrt{r^2 - 1}$ by $\sqrt{1 - r^2}$ in its four occurrences in the expression (19). Then we fix the overall sign of the full integral so that the leading term matches the sign of the leading term $\int_0^1 \frac{rdr}{\sqrt{1-r^2}}$ in (11) which is the pure dS_4 hemisphere area in (4), (5). This is the form of the area integral in (20) in the r -coordinate. Evaluating these at the various limiting points gives

$$I^>(r) \Big|_1^{R_c/l} = -i\frac{R_c}{l} + \epsilon \left(1 - i\frac{R_c}{l} \log \frac{R_c}{l} + i\frac{7}{6} \frac{R_c}{l} \right) - \frac{5}{3}\epsilon, \\ I^<(r) \Big|_0^1 = -\frac{5}{3}\epsilon - \left[-1 + \epsilon \left(\frac{7}{6} - i\pi - \log 4 \right) \right], \quad (74)$$

apart from singular terms at $r = 1$ which can be removed by the contour integral $I_\epsilon^\theta(r)$ around the regulating semicircle. The above pieces alongwith the overall $\frac{\pi l^2}{2G_4}$ factor add up to give (21).

C Details: dS_3 slow-roll area

In this dS_3 case we have

$$\beta(r) = -\frac{1}{2} \left(r \frac{\partial \varphi}{\partial r} \right)^2 + \frac{\varphi r^2}{1 - r^2}. \quad (75)$$

Inputting the scalar profile (63) in this case and using $r = \cosh \tau$ gives

$$\begin{aligned} \beta_{>}(r) = \frac{1}{32r^2(r^2-1)} & \left[-4r^4(1+\log 16) + 4r^2 - 4\log^2(r+\sqrt{r^2-1}) \right. \\ & + 4(2r\sqrt{r^2-1}(2r^2-1) + i\pi) \log(r+\sqrt{r^2-1}) \\ & \left. - 4i\pi(-2r^4 - r\sqrt{r^2-1} + 2r^3\sqrt{r^2-1}) + \pi^2 \right]. \end{aligned} \quad (76)$$

In terms of the variable $z = r^2 - 1$ in (13), this becomes

$$\begin{aligned} \beta_{>}(z) = \frac{1}{32z(z+1)} & \left[-4(z+1)^2(1+\log 16) + 4(z+1) - 4\log^2(\sqrt{z}+\sqrt{z+1}) \right. \\ & + 4(2\sqrt{z}\sqrt{z+1}(2(z+1)-1) + i\pi) \log(\sqrt{z}+\sqrt{z+1}) \\ & \left. - 4i\pi(2\sqrt{z}(z+1)^{3/2} - 2(z+1)^2 - \sqrt{z}\sqrt{z+1}) + \pi^2 \right]. \end{aligned} \quad (77)$$

Integrating gives

$$\begin{aligned} I_{\epsilon}^{>} = \int \frac{\beta_{>}(z)}{2i\sqrt{z(1+z)}} dz = \frac{1}{32\sqrt{z(z+1)}} & \left[i(8i\pi(z+1) - 4(2z+1)\log^2(\sqrt{z}+\sqrt{z+1}) \right. \\ & + \pi^2(2z+1) + 4i(2\pi z + \pi) \log(\sqrt{z}+\sqrt{z+1}) - 4(z+1)\log 16) \\ & \left. + 4\sqrt{z}\sqrt{z+1}(2\pi + i(1+\log 16)) \log(\sqrt{z}+\sqrt{z+1}) \right]. \end{aligned} \quad (78)$$

Along the lines of the arguments in (67) in the dS_4 case, we have

$$\int_{-1}^{-\delta} \frac{\beta_{>}(z)}{2\sqrt{-z(1+z)}} dz = \int_1^{\delta} \frac{\beta_{>}(-y)}{2\sqrt{y(1-y)}} d(-y) = \int_{\delta}^1 \frac{\beta_{<}(y)}{2\sqrt{y(1-y)}} dy \equiv I_{\epsilon}^{<}(z). \quad (79)$$

Thus, analytically continuing the integrated expression $I_{\epsilon}^{>}$ to the hemisphere region ($r < 1$) as $z \rightarrow -z$ gives

$$\begin{aligned} I_{\epsilon}^{<}(z) = I_{\epsilon}^{>}(-z) = \frac{1}{32\sqrt{z(1-z)}} & \left[(8i\pi(1-z) - 4(-2z+1)\log^2(i\sqrt{z}+\sqrt{1-z}) \right. \\ & + \pi^2(-2z+1) + 4i(-2\pi z + \pi) \log(i\sqrt{z}+\sqrt{1-z}) - 4(1-z)\log 16) \\ & \left. + 4\sqrt{z}\sqrt{1-z}(2\pi + i(1+\log 16)) \log(i\sqrt{z}+\sqrt{1-z}) \right]. \end{aligned} \quad (80)$$

Evaluating this at the various limiting points gives

$$\begin{aligned} z = z_c \rightarrow \infty : \quad I_{\epsilon}^{>} &= \frac{1}{16}i(-(\log z_c)^2 + \log z_c + \pi^2 + 4i\pi + 4(\log 2)^2 - 6\log 2), \\ z = \delta : \quad I_{\epsilon}^{>} &= -\frac{\pi}{8} + \frac{i(8i\pi + \pi^2 - 4\log 16)}{32\sqrt{\delta}}. \end{aligned} \quad (81)$$

Evaluating this now at $z = 1$ (nbp) and $z = \delta$ (which is 0^- in the earlier variable) gives

$$z = 1 : I_{\epsilon}^{<} = \frac{\pi}{16}(2\pi i - 1 - \log 16); \quad z = \delta : I_{\epsilon}^{<} = -\frac{\pi}{8} + \frac{(8i\pi + \pi^2 - 4\log(16))}{32\sqrt{\delta}}. \quad (82)$$

The contribution on the regulating semicircle is similar to that in the dS_4 case and serves to cancel the singular pieces near $z = 0$: we obtain

$$I_\epsilon^\theta = -\frac{(8i\pi + \pi^2 - 4 \log 16)}{32\sqrt{-\delta} e^{i\theta}} \Big|_{\theta=\pi}^{\theta=0} = -\frac{(8i\pi + \pi^2 - 4 \log 16)}{32\sqrt{\delta}} \left(\frac{1}{i} - 1 \right). \quad (83)$$

Adding all these above contributions leads to (29). As in the dS_4 case, this area calculation can be done in the r -coordinate also, using (76), and its continuation to the hemisphere.

D Inflation: on-shell action etc

We review aspects of evaluating the action for spaces with a boundary: besides [48, 50, 51], and [49], some useful references include [10, 52, 53, 54, 55, 56] We consider the $d + 1$ -dim Einstein-scalar action

$$I = \frac{1}{16\pi G_{d+1}} \int d^{d+1}x \sqrt{g} (R - (\partial\phi)^2 - 2V(\phi)) - \frac{1}{8\pi G_{d+1}} \int d^3x \sqrt{h} K. \quad (84)$$

With a minisuperspace-type metric ansatz as required for our analysis here

$$ds^2 = -N^2(t)dt^2 + a^2(t)d\Omega_d^2, \quad (85)$$

and a $d + 1$ -split in the ADM formulation, we obtain the spatial curvature and the extrinsic curvature as

$$R^{(d)} = \frac{d(d-1)}{a^2}, \quad K_{ij} = \frac{1}{2N} \dot{h}_{ij} = \frac{1}{2N} 2a\dot{a} s_{ij}, \quad K = s^{ij} K_{ij} = \frac{d\dot{a}}{aN}, \quad (86)$$

where s_{ij} is the unit S^d metric. Alongwith cancellations between the bulk and boundary terms above, this gives the Lorentzian action

$$\begin{aligned} iI &= \frac{i}{16\pi G_{d+1}} \int dt \Omega_d N a^d \left(K_{ij} K^{ij} - K^2 + R^{(d)} - 2V + \frac{1}{N^2} \dot{\phi}^2 \right) \\ &= \frac{i\Omega_d}{16\pi G_{d+1}} \int dt N a^d \left(-d(d-1) \frac{\dot{a}^2}{a^2 N^2} + d(d-1) \frac{1}{a^2} - 2V + \frac{1}{N^2} \dot{\phi}^2 \right). \end{aligned} \quad (87)$$

Varying with N leads to the Hamiltonian constraint with Lorentzian signature:

$$R^{(d)} - 2V - \frac{1}{N^2} K_{ij} K^{ij} + \frac{1}{N^2} K^2 - \frac{1}{N^2} \dot{\phi}^2 = 0 = \frac{d(d-1)}{a^2} + d(d-1) \frac{\dot{a}^2}{a^2 N^2} - 2V - \frac{1}{N^2} \dot{\phi}^2. \quad (88)$$

To go Euclidean, we either take $N \rightarrow iN$ or $t \rightarrow it$ so $-N^2 dt^2 \rightarrow N^2 dt^2$. This gives

$$-I_E = \frac{\Omega_d}{16\pi G_{d+1}} \int dt N a^d \left(d(d-1) \frac{\dot{a}^2}{a^2 N^2} + d(d-1) \frac{1}{a^2} - 2V - \frac{1}{N^2} \dot{\phi}^2 \right), \quad (89)$$

as the Euclidean action and the Hamiltonian constraint becomes

$$\frac{d(d-1)}{a^2} - 2V - d(d-1)\frac{\dot{a}^2}{a^2 N^2} + \frac{1}{N^2}\dot{\phi}^2 = 0. \quad (90)$$

For the metric in the Euclidean form on the right in (7), with a taken as the time coordinate so $\dot{a} = 1$, we then obtain

$$g_{aa} \equiv N^2 = \frac{\frac{d(d-1)}{2} - \frac{1}{2}(a\partial_a\phi)^2}{\frac{d(d-1)}{2} - V a^2}. \quad (91)$$

Inputting the Hamiltonian constraint, we can evaluate the on-shell action with the time coordinate taken as $a = t$. We will now evaluate this for dS_4 and dS_3 slow-roll inflation to $O(\epsilon)$ in the slow-roll parameter.

dS_4 slow-roll:

With $d = 3$, inputting the Hamiltonian constraint, we obtain the on-shell action

$$-I_E = \frac{6\Omega_3}{16\pi G_4} \int da N a \left(\frac{1}{N^2} + 1 - \frac{a^2\dot{\phi}^2}{6N^2} - \frac{a^2V}{3} \right) = \frac{3\pi}{2G_4} \int da N a \left(1 - \frac{a^2V}{3} \right). \quad (92)$$

Thus the Lorentzian action taking $N^2 \rightarrow -N^2$ can be written with the minus sign inside one radical and becomes

$$iI = -\frac{i\pi}{2G_4} \int da a \sqrt{3 - \frac{1}{2}(a\partial_a\phi)^2} \sqrt{a^2V - 3}. \quad (93)$$

For pure dS_4 , we have $V \equiv \Lambda = \frac{3}{l^2}$ and $\phi = \text{const}$, giving the real part of the action as $\text{Re}(iI) = -\frac{3i\pi l^2}{2G_4} \int_0^1 dr r \sqrt{r^2 - 1} = \frac{\pi l^2}{2G_4}$, *i.e.* half dS_4 entropy as expected.

Incorporating the slow-roll correction and expanding to $O(\epsilon)$, we obtain

$$iI = -\frac{3i\pi l^2}{2G_4} \int_0^{r_c} dr r \sqrt{r^2 - 1} \left[1 + \epsilon \left(-\frac{1}{6} (r\partial_r\tilde{\varphi}(r))^2 + \frac{r^2\tilde{\varphi}(r)}{r^2 - 1} \right) \right]. \quad (94)$$

Breaking up the integral into the Euclidean part over $r \in [0, 1]$ and the Lorentzian part $r \in [1, r_c]$ with $r_c \equiv \frac{R_c}{l}$, the leading pure de Sitter term gives

$$iI_0 = \frac{\pi l^2}{2G_4} \left[1 - i \left(r_c^3 - \frac{3}{2}r_c + O\left(\frac{1}{r_c}\right) \right) \right]. \quad (95)$$

For the $O(\epsilon)$ correction, we use the explicit expressions for the inflaton profile and evaluate (*e.g.* by defining an appropriate contour to avoid the pole at $r = 1$). Simplifying finally gives

$$iI_\epsilon = \frac{\pi l^2}{2G_4} \epsilon \left[ir_c^3 \left(\log r_c - \frac{1}{6} \right) + \frac{ir_c}{4} (6 \log r_c - 11) + \left(\log 4 - \frac{7}{2} + i\pi \right) + O\left(\frac{1}{r_c}\right) \right]. \quad (96)$$

This recovers the expressions in [49] (see App.C.1 for the $O(\epsilon)$ terms), after noting $\frac{V_*}{3} = l^2$ and reinstating $8\pi G_4$.

dS_3 slow-roll:

With $d = 2$, inputting the Hamiltonian constraint gives $I_E = -\frac{2\Omega_2}{8\pi G_4} \int da N (1 - a^2 V)$, so the on-shell Lorentzian action becomes

$$iI = -\frac{i}{G_3} \int da a \sqrt{1 - \frac{1}{2}(a\partial_a\phi)^2} \sqrt{a^2 V - 1}. \quad (97)$$

Expanding to $O(\epsilon)$ and simplifying gives

$$iI = -\frac{il}{G_3} \int_0^{r_c} dr \sqrt{r^2 - 1} \left[1 + \epsilon \left(-\frac{1}{2} (r\partial_r \tilde{\varphi}(r))^2 + \frac{r^2 \tilde{\varphi}(r)}{r^2 - 1} \right) \right]. \quad (98)$$

The leading term is the pure dS_3 action

$$\begin{aligned} iI_0 &= -\frac{il}{G_3} \left[\frac{i\pi}{4} + \frac{1}{2} \left(r_c \sqrt{r_c^2 - 1} - \log \left(r_c + \sqrt{r_c^2 - 1} \right) \right) \right] \\ &= \frac{\pi l}{4G_3} - \frac{il}{G_3} \left(\frac{r_c^2}{2} - \frac{1}{2} \log r_c - \frac{1}{2} \log 2 - \frac{1}{4} \right) + O\left(\frac{1}{r_c}\right). \end{aligned} \quad (99)$$

The subleading $O(\epsilon)$ terms can be evaluated as in the dS_4 case (*e.g.* by an appropriate contour in the complex r -plane, avoiding the pole at $r = 1$). Simplifying, this finally gives

$$\begin{aligned} iI_\epsilon &= \frac{l}{2G_3} \epsilon \left[-\frac{\pi}{16} (1 + \log 16) \right. \\ &\quad \left. + \frac{i}{16} (4z_c \log z_c - 2z_c + (\log z_c)^2 + \log z_c + \pi^2 + 1 - 4(\log 2)^2 - 2 \log 2) \right]. \end{aligned} \quad (100)$$

Using $z_c = r_c^2 - 1$ and expanding gives

$$\begin{aligned} iI_\epsilon &= \frac{l}{2G_3} \epsilon \left[-\frac{\pi}{16} (1 + \log 16) \right. \\ &\quad \left. + \frac{i}{16} (8r_c^2 \log r_c - 2r_c^2 + 4(\log r_c)^2 - 6 \log r_c + \pi^2 - 1 - 4(\log 2)^2 - 2 \log 2) \right]. \end{aligned} \quad (101)$$

References

- [1] J. M. Maldacena, “The large N limit of superconformal field theories and supergravity,” *Adv. Theor. Math. Phys.* **2**, 231 (1998) [*Int. J. Theor. Phys.* **38**, 1113 (1999)] [arXiv:hep-th/9711200].
- [2] S. S. Gubser, I. R. Klebanov and A. M. Polyakov, “Gauge theory correlators from non-critical string theory,” *Phys. Lett. B* **428**, 105 (1998) [arXiv:hep-th/9802109].

- [3] E. Witten, “Anti-de Sitter space and holography,” *Adv. Theor. Math. Phys.* **2**, 253 (1998) [arXiv:hep-th/9802150].
- [4] S. Ryu and T. Takayanagi, “Holographic derivation of entanglement entropy from AdS/CFT,” *Phys. Rev. Lett.* **96**, 181602 (2006) [hep-th/0603001].
- [5] S. Ryu and T. Takayanagi, “Aspects of Holographic Entanglement Entropy,” *JHEP* **0608**, 045 (2006) [hep-th/0605073].
- [6] V. E. Hubeny, M. Rangamani and T. Takayanagi, “A Covariant holographic entanglement entropy proposal,” *JHEP* **0707** (2007) 062 [arXiv:0705.0016 [hep-th]].
- [7] M. Rangamani and T. Takayanagi, “Holographic Entanglement Entropy,” *Lect. Notes Phys.* **931**, pp.1-246 (2017) Springer, 2017, doi:10.1007/978-3-319-52573-0 [arXiv:1609.01287 [hep-th]].
- [8] A. Strominger, “The dS / CFT correspondence,” *JHEP* **0110**, 034 (2001) [hep-th/0106113].
- [9] E. Witten, “Quantum gravity in de Sitter space,” [hep-th/0106109].
- [10] J. M. Maldacena, “Non-Gaussian features of primordial fluctuations in single field inflationary models,” *JHEP* **0305**, 013 (2003), [astro-ph/0210603].
- [11] D. Anninos, T. Hartman and A. Strominger, “Higher Spin Realization of the dS/CFT Correspondence,” *Class. Quant. Grav.* **34**, no. 1, 015009 (2017) doi:10.1088/1361-6382/34/1/015009 [arXiv:1108.5735 [hep-th]].
- [12] M. Spradlin, A. Strominger and A. Volovich, “Les Houches lectures on de Sitter space,” hep-th/0110007.
- [13] D. Anninos, “De Sitter Musings,” *Int. J. Mod. Phys. A* **27**, 1230013 (2012) doi:10.1142/S0217751X1230013X [arXiv:1205.3855 [hep-th]].
- [14] D. A. Galante, “Modave lectures on de Sitter space & holography,” *PoS Modave2022*, 003 (2023) doi:10.22323/1.435.0003 [arXiv:2306.10141 [hep-th]].
- [15] G. W. Gibbons and S. W. Hawking, “Cosmological Event Horizons, Thermodynamics, and Particle Creation,” *Phys. Rev. D* **15**, 2738 (1977). doi:10.1103/PhysRevD.15.2738
- [16] K. Narayan, “de Sitter extremal surfaces,” *Phys. Rev. D* **91**, no. 12, 126011 (2015) [arXiv:1501.03019 [hep-th]].
- [17] K. Narayan, “de Sitter space and extremal surfaces for spheres,” *Phys. Lett. B* **753**, 308 (2016) [arXiv:1504.07430 [hep-th]].
- [18] Y. Sato, “Comments on Entanglement Entropy in the dS/CFT Correspondence,” *Phys. Rev. D* **91**, no. 8, 086009 (2015) [arXiv:1501.04903 [hep-th]].
- [19] M. Miyaji and T. Takayanagi, “Surface/State Correspondence as a Generalized Holography,” *PTEP* **2015**, no. 7, 073B03 (2015) doi:10.1093/ptep/ptv089 [arXiv:1503.03542 [hep-th]].

- [20] K. Narayan, “On extremal surfaces and de Sitter entropy,” *Phys. Lett. B* **779**, 214 (2018) [arXiv:1711.01107 [hep-th]].
- [21] K. Narayan, “de Sitter entropy as entanglement,” *Int. J. Mod. Phys. D* **28**, no.14, 1944019 (2019) doi:10.1142/S021827181944019X [arXiv:1904.01223 [hep-th]].
- [22] K. Narayan, “de Sitter future-past extremal surfaces and the entanglement wedge,” *Phys. Rev. D* **101**, no.8, 086014 (2020) doi:10.1103/PhysRevD.101.086014 [arXiv:2002.11950 [hep-th]].
- [23] K. Doi, J. Harper, A. Mollabashi, T. Takayanagi and Y. Taki, “Pseudoentropy in dS/CFT and Timelike Entanglement Entropy,” *Phys. Rev. Lett.* **130**, no.3, 031601 (2023) doi:10.1103/PhysRevLett.130.031601 [arXiv:2210.09457 [hep-th]].
- [24] K. Narayan, “de Sitter space, extremal surfaces, and time entanglement,” *Phys. Rev. D* **107**, no.12, 126004 (2023) doi:10.1103/PhysRevD.107.126004 [arXiv:2210.12963 [hep-th]].
- [25] K. Narayan, “Further remarks on de Sitter space, extremal surfaces, and time entanglement,” *Phys. Rev. D* **109**, no.8, 086009 (2024) doi:10.1103/PhysRevD.109.086009 [arXiv:2310.00320 [hep-th]].
- [26] Y. Hikida, T. Nishioka, T. Takayanagi and Y. Taki, “CFT duals of three-dimensional de Sitter gravity,” *JHEP* **05**, 129 (2022) doi:10.1007/JHEP05(2022)129 [arXiv:2203.02852 [hep-th]].
- [27] Y. Hikida, T. Nishioka, T. Takayanagi and Y. Taki, “Holography in de Sitter Space via Chern-Simons Gauge Theory,” *Phys. Rev. Lett.* **129**, no.4, 041601 (2022) [arXiv:2110.03197 [hep-th]].
- [28] J. Cotler and A. Strominger, “Cosmic ER=EPR in dS/CFT,” [arXiv:2302.00632 [hep-th]].
- [29] Y. Nakata, T. Takayanagi, Y. Taki, K. Tamaoka and Z. Wei, “New holographic generalization of entanglement entropy,” *Phys. Rev. D* **103**, no.2, 026005 (2021) [arXiv:2005.13801 [hep-th]].
- [30] Z. Li, Z. Q. Xiao and R. Q. Yang, “On holographic time-like entanglement entropy,” *JHEP* **04**, 004 (2023) doi:10.1007/JHEP04(2023)004 [arXiv:2211.14883 [hep-th]].
- [31] K. Doi, J. Harper, A. Mollabashi, T. Takayanagi and Y. Taki, “Timelike entanglement entropy,” *JHEP* **05**, 052 (2023) doi:10.1007/JHEP05(2023)052 [arXiv:2302.11695 [hep-th]].
- [32] X. Jiang, P. Wang, H. Wu and H. Yang, “Timelike entanglement entropy and TT^- deformation,” *Phys. Rev. D* **108**, no.4, 046004 (2023) doi:10.1103/PhysRevD.108.046004 [arXiv:2302.13872 [hep-th]].
- [33] Z. Chen, “Complex-valued Holographic Pseudo Entropy via Real-time AdS/CFT Correspondence,” [arXiv:2302.14303 [hep-th]].
- [34] X. Jiang, P. Wang, H. Wu and H. Yang, “Timelike entanglement entropy in dS_3/CFT_2 ,” *JHEP* **08**, 216 (2023) doi:10.1007/JHEP08(2023)216 [arXiv:2304.10376 [hep-th]].
- [35] C. S. Chu and H. Parihar, “Time-like entanglement entropy in AdS/BCFT,” *JHEP* **06**, 173 (2023) doi:10.1007/JHEP06(2023)173 [arXiv:2304.10907 [hep-th]].
- [36] H. Y. Chen, Y. Hikida, Y. Taki and T. Uetoko, “Complex saddles of Chern-Simons gravity and dS_3/CFT_2 correspondence,” *Phys. Rev. D* **108**, no.6, 066005 (2023) [arXiv:2306.03330 [hep-th]].

- [37] D. Chen, X. Jiang and H. Yang, “Holographic $T\bar{T}$ deformed entanglement entropy in dS_3/CFT_2 ,” [arXiv:2307.04673 [hep-th]].
- [38] P. Z. He and H. Q. Zhang, “Timelike Entanglement Entropy from Rindler Method,” [arXiv:2307.09803 [hep-th]].
- [39] A. Das, S. Sachdeva and D. Sarkar, “Bulk reconstruction using timelike entanglement in (A)dS,” Phys. Rev. D **109**, no.6, 066007 (2024) doi:10.1103/PhysRevD.109.066007 [arXiv:2312.16056 [hep-th]].
- [40] D. Basu and V. Raj, “Reflected entropy and timelike entanglement in TT^- -deformed CFTs,” Phys. Rev. D **110**, no.4, 046009 (2024) doi:10.1103/PhysRevD.110.046009 [arXiv:2402.07253 [hep-th]].
- [41] R. Fareghbal, “Flat-space limit of holographic pseudoentropy in (A)dS spacetimes,” Phys. Rev. D **110**, no.6, 066019 (2024) doi:10.1103/PhysRevD.110.066019 [arXiv:2408.03061 [hep-th]].
- [42] M. P. Heller, F. Ori and A. Serantes, “Geometric interpretation of timelike entanglement entropy,” [arXiv:2408.15752 [hep-th]].
- [43] A. Lewkowycz and J. Maldacena, “Generalized gravitational entropy,” JHEP **08**, 090 (2013) doi:10.1007/JHEP08(2013)090 [arXiv:1304.4926 [hep-th]].
- [44] X. Dong, A. Lewkowycz and M. Rangamani, “Deriving covariant holographic entanglement,” JHEP **11**, 028 (2016) doi:10.1007/JHEP11(2016)028 [arXiv:1607.07506 [hep-th]].
- [45] X. Dong, “The Gravity Dual of Renyi Entropy,” Nature Commun. **7**, 12472 (2016) doi:10.1038/ncomms12472 [arXiv:1601.06788 [hep-th]].
- [46] X. Dong, “Holographic Entanglement Entropy for General Higher Derivative Gravity,” JHEP **01**, 044 (2014) doi:10.1007/JHEP01(2014)044 [arXiv:1310.5713 [hep-th]].
- [47] H. Casini, M. Huerta and R. C. Myers, “Towards a derivation of holographic entanglement entropy,” JHEP **1105**, 036 (2011) [arXiv:1102.0440 [hep-th]].
- [48] J. B. Hartle and S. W. Hawking, “Wave Function of the Universe,” Phys. Rev. D **28**, 2960-2975 (1983) doi:10.1103/PhysRevD.28.2960
- [49] J. Maldacena, “Comments on the no boundary wavefunction and slow roll inflation,” [arXiv:2403.10510 [hep-th]].
- [50] R. Bousso and S. W. Hawking, “The Probability for primordial black holes,” Phys. Rev. D **52**, 5659-5664 (1995) doi:10.1103/PhysRevD.52.5659 [arXiv:gr-qc/9506047 [gr-qc]].
- [51] R. Bousso and S. W. Hawking, “Pair creation of black holes during inflation,” Phys. Rev. D **54**, 6312-6322 (1996) doi:10.1103/PhysRevD.54.6312 [arXiv:gr-qc/9606052 [gr-qc]].
- [52] J. B. Hartle, S. W. Hawking and T. Hertog, “The Classical Universes of the No-Boundary Quantum State,” Phys. Rev. D **77**, 123537 (2008) doi:10.1103/PhysRevD.77.123537 [arXiv:0803.1663 [hep-th]].

- [53] J. Diaz Dorronsoro, J. J. Halliwell, J. B. Hartle, T. Hertog and O. Janssen, “Real no-boundary wave function in Lorentzian quantum cosmology,” *Phys. Rev. D* **96**, no.4, 043505 (2017) doi:10.1103/PhysRevD.96.043505 [arXiv:1705.05340 [gr-qc]].
- [54] J. J. Halliwell, J. B. Hartle and T. Hertog, “What is the No-Boundary Wave Function of the Universe?,” *Phys. Rev. D* **99**, no.4, 043526 (2019) doi:10.1103/PhysRevD.99.043526 [arXiv:1812.01760 [hep-th]].
- [55] J. Maldacena, G. J. Turiaci and Z. Yang, “Two dimensional Nearly de Sitter gravity,” *JHEP* **01**, 139 (2021) doi:10.1007/JHEP01(2021)139 [arXiv:1904.01911 [hep-th]].
- [56] O. Janssen, “Slow-roll approximation in quantum cosmology,” *Class. Quant. Grav.* **38**, no.9, 095003 (2021) doi:10.1088/1361-6382/abe143 [arXiv:2009.06282 [gr-qc]].
- [57] T. Hertog, O. Janssen and J. Karlsson, “Kontsevich-Segal Criterion in the No-Boundary State Constrains Inflation,” *Phys. Rev. Lett.* **131**, no.19, 191501 (2023) doi:10.1103/PhysRevLett.131.191501 [arXiv:2305.15440 [hep-th]].
- [58] G. W. Gibbons and S. W. Hawking, “Action Integrals and Partition Functions in Quantum Gravity,” *Phys. Rev. D* **15**, 2752-2756 (1977) doi:10.1103/PhysRevD.15.2752
- [59] S. W. Hawking and D. N. Page, “Thermodynamics of Black Holes in anti-De Sitter Space,” *Commun. Math. Phys.* **87**, 577 (1983) doi:10.1007/BF01208266
- [60] E. Witten, “Anti-de Sitter space, thermal phase transition, and confinement in gauge theories,” *Adv. Theor. Math. Phys.* **2**, 505-532 (1998) doi:10.4310/ATMP.1998.v2.n3.a3 [arXiv:hep-th/9803131 [hep-th]].
- [61] T. Hartman and J. Maldacena, “Time Evolution of Entanglement Entropy from Black Hole Interiors,” *JHEP* **1305**, 014 (2013) [arXiv:1303.1080 [hep-th]].
- [62] J. M. Maldacena, “Eternal black holes in anti-de Sitter,” *JHEP* **0304**, 021 (2003) [hep-th/0106112].
- [63] K. Narayan, “On dS_4 extremal surfaces and entanglement entropy in some ghost CFTs,” *Phys. Rev. D* **94**, no. 4, 046001 (2016) [arXiv:1602.06505 [hep-th]].
- [64] D. P. Jatkar and K. Narayan, “Ghost-spin chains, entanglement and bc -ghost CFTs,” *Phys. Rev. D* **96**, no. 10, 106015 (2017) [arXiv:1706.06828 [hep-th]].
- [65] K. Doi, N. Ogawa, K. Shinmyo, Y. k. Suzuki and T. Takayanagi, “Probing de Sitter Space Using CFT States,” [arXiv:2405.14237 [hep-th]].
- [66] D. Baumann, “Inflation,” doi:10.1142/9789814327183_0010 [arXiv:0907.5424 [hep-th]].
- [67] D. Baumann and L. McAllister, “Inflation and String Theory,” Cambridge University Press, 2015, ISBN 978-1-107-08969-3, 978-1-316-23718-2 doi:10.1017/CBO9781316105733 [arXiv:1404.2601 [hep-th]].
- [68] N. Ogawa, T. Takayanagi and T. Ugajin, “Holographic Fermi Surfaces and Entanglement Entropy,” *JHEP* **1201**, 125 (2012) [arXiv:1111.1023 [hep-th]].
- [69] L. Huijse, S. Sachdev and B. Swingle, “Hidden Fermi surfaces in compressible states of gauge-gravity duality,” *Phys. Rev. B* **85**, 035121 (2012) [arXiv:1112.0573 [cond-mat.str-el]].

- [70] X. Dong, S. Harrison, S. Kachru, G. Torroba and H. Wang, “Aspects of holography for theories with hyperscaling violation,” *JHEP* **1206**, 041 (2012) [arXiv:1201.1905 [hep-th]].
- [71] K. Narayan, “On Lifshitz scaling and hyperscaling violation in string theory,” *Phys. Rev. D* **85**, 106006 (2012) [arXiv:1202.5935 [hep-th]].
- [72] K. Narayan, T. Takayanagi and S. P. Trivedi, “AdS plane waves and entanglement entropy,” *JHEP* **1304**, 051 (2013) [arXiv:1212.4328 [hep-th]].
- [73] K. Narayan, “On a lightlike limit of entanglement,” *Phys. Rev. D* **91**, no.8, 086010 (2015) doi:10.1103/PhysRevD.91.086010 [arXiv:1408.7021 [hep-th]].
- [74] K. Fernandes, K. S. Kolekar, K. Narayan and S. Roy, “Schwarzschild de Sitter and extremal surfaces,” *Eur. Phys. J. C* **80**, no.9, 866 (2020) doi:10.1140/epjc/s10052-020-08437-2 [arXiv:1910.11788 [hep-th]].
- [75] K. Goswami and K. Narayan, “Small Schwarzschild de Sitter black holes, quantum extremal surfaces and islands,” *JHEP* **10**, 031 (2022) doi:10.1007/JHEP10(2022)031 [arXiv:2207.10724 [hep-th]].
- [76] K. Goswami and K. Narayan, “Small Schwarzschild de Sitter black holes, the future boundary and islands,” *JHEP* **05**, 016 (2024) doi:10.1007/JHEP05(2024)016 [arXiv:2312.05904 [hep-th]].
- [77] E. K. Morvan, J. P. van der Schaar and M. R. Visser, “On the Euclidean action of de Sitter black holes and constrained instantons,” *SciPost Phys.* **14**, no.2, 022 (2023) doi:10.21468/SciPostPhys.14.2.022 [arXiv:2203.06155 [hep-th]].
- [78] M. Kontsevich and G. Segal, “Wick Rotation and the Positivity of Energy in Quantum Field Theory,” *Quart. J. Math. Oxford Ser.* **72**, no.1-2, 673-699 (2021) doi:10.1093/qmath/haab027 [arXiv:2105.10161 [hep-th]].
- [79] E. Witten, “A Note On Complex Spacetime Metrics,” [arXiv:2111.06514 [hep-th]].
- [80] I. Mata, S. Raju and S. Trivedi, “CMB from CFT,” *JHEP* **07**, 015 (2013) doi:10.1007/JHEP07(2013)015 [arXiv:1211.5482 [hep-th]].
- [81] A. Ghosh, N. Kundu, S. Raju and S. P. Trivedi, “Conformal Invariance and the Four Point Scalar Correlator in Slow-Roll Inflation,” *JHEP* **07**, 011 (2014) doi:10.1007/JHEP07(2014)011 [arXiv:1401.1426 [hep-th]].
- [82] I. Dey, K. K. Nanda, A. Roy and S. P. Trivedi, “Aspects of dS/CFT Holography,” [arXiv:2407.02417 [hep-th]].